Structure of Southern Ocean fronts at 140°E

Serguei Sokolov*, Stephen R. Rintoul

CSIRO Marine Research and Antarctic CRC, GPO Box 1538, Hobart, Tasmania, Australia

Abstract

The major fronts between Tasmania and Antarctica are described on the basis of repeat hydrographic and expendable bathythermograph (XBT) sections and satellite altimetry. The high spatial and temporal resolution allows the location, structure and variability of the fronts to be investigated in detail. A large number of criteria are examined in an effort to identify reliable indicators of the fronts (e.g. lateral gradients along isobars and isopycnals, transport maxima, and the latitude where a property isoline crosses a particular isobar). The location of the Subtropical Front (STF) varies by less than 1° from its mean latitude of 45.2°S between the Tasmanian continental slope and the South Tasman Rise. The high resolution sections resolve multiple branches or filaments of each of the main fronts of the Antarctic Circumpolar Current (ACC) south of Australia: the Subantarctic Front (SAF) has two cores at mean latitudes of 50.5° and 52°S, the Polar Front (PF) has two branches which are found between 53° and 54°S and between 59° and 60°S, and the southern ACC front crosses the section near 62°S and 64°S. The southern boundary of the ACC sometimes merges with the southern ACC front (SACCF). The Antarctic Slope Front is found over the upper continental slope on those sections, which extend sufficiently close to Antarctica. Each of the frontal filaments identified on the repeat sections corresponds to a narrow range of sea surface height (SSH) values. These SSH streamlines are also found to correspond to large lateral gradients of SSH (i.e. fronts) east and west of the repeat section. Maps of sea surface height are then used to determine the path and variability of the fronts. The maps confirm the multi-filament structure of the fronts and show that streamlines merge and split along the path of the fronts. Each of the ACC fronts extends throughout the water column; as a result, the path of the fronts and the width of their meander envelopes are strongly influenced by bathymetry. Meridional displacements of the fronts are correlated with variations in SST, suggesting shifts of the fronts contribute to SST variability observed on interannual time scales.
© 2002 Elsevier Science B.V. All rights reserved.

Keywords: Subantarctic Front; Polar Front; Antarctic Circumpolar Current; Southern Ocean; Satellite altimetry; Australian sector (130–160°E)

1. Introduction

Deacon (1937) was the first to note that the transition from warm, light subtropical water in the north to cold, dense Antarctic water in the south occurred in a step-like manner, rather than as a gradual change across the breadth of the Southern Ocean. Subsequent voyages with more closely spaced

---

* Corresponding author. Tel.: +61-3-6232-5218; fax: +61-3-6232-5123.

E-mail addresses: serguei.sokolov@marine.csiro.au (S. Sokolov), steve.rintoul@marine.csiro.au (S.R. Rintoul).

stations confirmed that these bands of enhanced meridional gradient, or fronts, could be found throughout the Southern Ocean. Orsi et al. (1995) and Belkin and Gordon (1996) have recently used historical data to carefully map the circumpolar distribution of the Southern Ocean fronts. The fronts coincide with current cores, which carry most of the transport of the Antarctic Circumpolar Current (ACC) (Nowlin and Clifford, 1982). Between the fronts lie zones of relatively uniform water mass properties. From north to south, the fronts and zones of the Southern Ocean are: the Subtropical Front (STF), Subantarctic Zone (SAZ), Subantarctic Front (SAF), Polar Frontal Zone (PFZ), Polar Front (PF), and Antarctic Zone (AZ) (Whitworth, 1980).

Understanding the structure and location of the major fronts of the Southern Ocean is of considerable importance. The fact that the flow of the Antarctic Circumpolar Current is organized into a small number of relatively narrow, deep-reaching jets provides clues to the still poorly understood dynamics of the current (Nowlin and Klinck, 1986; Rintoul et al., in press(a)). The zones between the fronts tend to be populated by distinct biological communities. For example, the SAZ south of Tasmania is very low in silicate and the phytoplankton community is dominated by small nonsilicieous cells, while south of the PF surface waters are rich in silicate and diatoms dominate the phytoplankton community (Rintoul and Trull, submitted for publication; Trull et al., 2001). The fronts themselves are at least in some locations areas of higher productivity (e.g., de Baar, 1995).

A variety of definitions have been used to identify the fronts of the Southern Ocean (see Peterson and Stramma, 1991; Orsi et al., 1995; Belkin and Gordon, 1996 for useful summaries of these definitions). While it is clear that the major fronts are circumpolar in extent, it is also clear that the fronts are not identical in all sectors of the Southern Ocean. The variations in frontal structure from region to region and the multiplicity of definitions used by various authors have led to some confusion in identifying particular fronts. In addition, many areas, including the region south of Australia, have remained relatively poorly sampled. In even fewer locations have repeat measurements been made to permit the variability of the fronts to be assessed.

The aim of this paper is to use the comprehensive data set collected south of Tasmania during the last decade to determine the location, structure and variability of the major fronts in this region. The data set includes six high resolution full-depth hydrographic sections collected during the World Ocean Circulation Experiment (WOCE section SR3), 45 austral summer expendable bathythermograph (XBT) sections obtained between 1992 and 1999, and satellite altimetry. The repeat hydrographic measurements obtained on the SR3 line are used to define suitable proxies in the XBT and altimeter data, which allow the fronts to be located in these more continuous, but less complete, observations.

The paper is organized as follows. Section 2 describes the data sets used. Section 3 describes the methods used to identify the major fronts, using the January 1995 occupation of SR3 as an example. Maps of sea surface height are used in Section 4 to determine the mean position and variability of the fronts in the Tasmanian sector (130°E to 160°E). The interannual variability of the front locations, and its correlation with variations in sea surface temperature, is determined from a 7-year time series of XBT sections in Section 5. Implications of the results are discussed in Section 6, and Section 7 provides a summary.

2. Data

The WOCE SR3 repeat hydrographic section between Tasmania and Antarctica was occupied six times in different seasons between 1991 and 1996 (Table 1). Stations along SR3 were generally 56 km

Table 1
Occupations of the WOCE SR3 line by Aurora Australis

Cruise	Month, Year	Number of stations	Reference
au9101	October, 1991	24	Rintoul and Bullister (1999)
au9309	March, 1993	47	Rosenberg et al. (1995a)
au9407	January, 1994	53	Rosenberg et al. (1995b)
au9404	January, 1995	51	Rosenberg et al. (1996)
au9501	July, 1995	54	Rosenberg et al. (1997)
au9601	September, 1996	57	Rosenberg et al. (1997)

apart over the deep basins and more closely spaced over the Tasmanian and Antarctic continental slopes and across the fronts. The first occupation of SR3 in October 1991 had lower resolution due to extreme weather conditions (Rintoul and Bullister, 1999). On each station, a rosette sampler equipped with a CTD was lowered to within 10 m of the sea floor. Continuous profiles of temperature, salinity and oxygen

were obtained at each station, and water samples at 24 depths were analyzed for salinity, oxygen and nutrients. All data were labeled with the neutral density variable (Jackett and McDougall, 1997); density values quoted in the text are neutral density anomaly (γ_n), in units of $kg \times m^{-3}$. A description of nutrient, tracer and water mass distributions along the SR3 section during late winter of 1991 can be found in Rintoul and
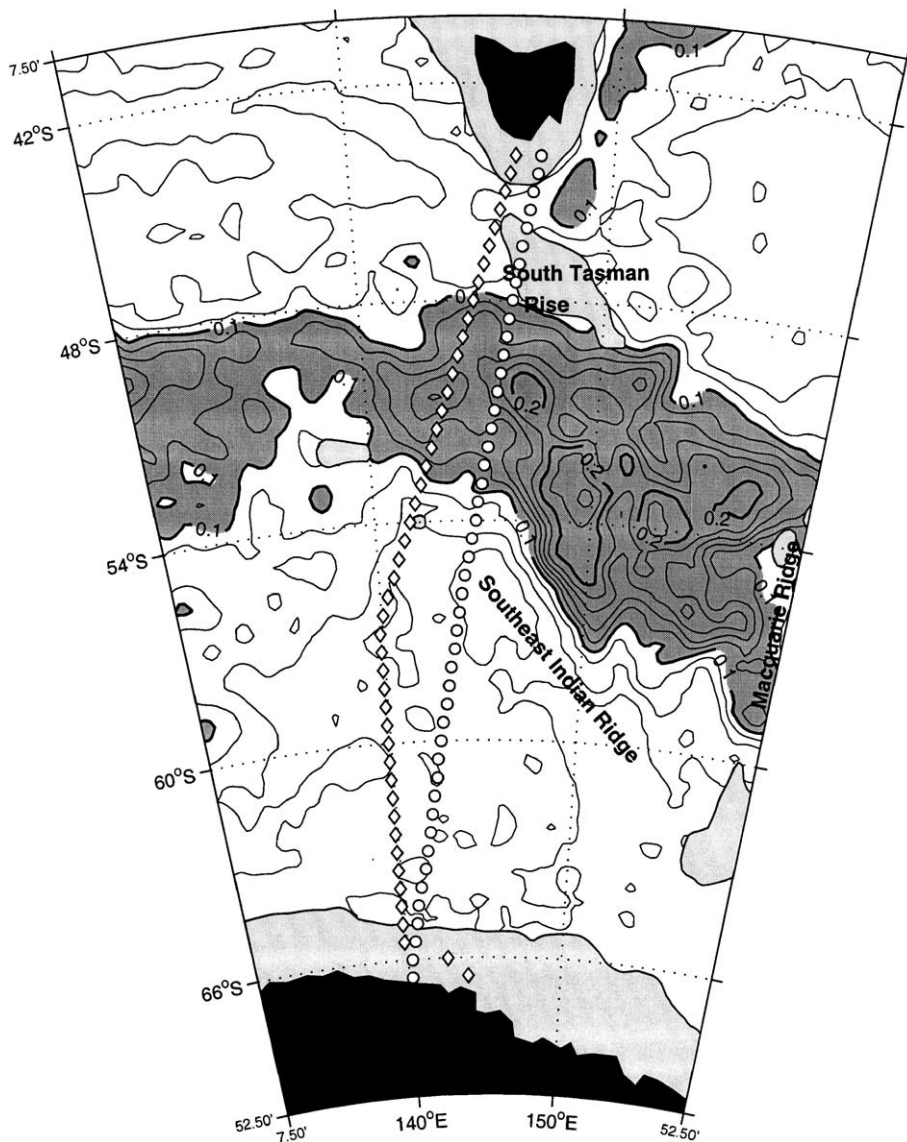

Fig. 1. Cruise track for WOCE SR3 repeat hydrographic section (diamonds) and Astrolabe repeat XBT line (circles). Depths shallower than 3500 m are light shaded. Contours are the standard deviation of sea surface height (in m).

Bullister (1999), and estimates of mass, heat, salt and nutrient fluxes for all SR3 repeats are reported in Rintoul and Sokolov (2001).

We use sea surface height (SSH) maps to identify fronts to the east and west of the SR3 line. Specifically, we used the CLS/AVISO "Mean Sea Level Anomaly" (MSLA) maps, which are produced by mapping data from the Topex/POSEIDON, ERS-1 and ERS-2 satellite altimeters (Le Traon et al., 1998). To produce maps of absolute SSH, we added the mean surface dynamic height (relative to 2500 dbar) from the Olbers et al. (1992) climatology. The climatology and the mean dynamic height estimated from the six repeats of SR3 agree well, although the climatology is somewhat smoother (not shown). In Section 4, we demonstrate that the SSH maps con-

structed in this way correspond closely to the density distribution measured along SR3.

To estimate the interannual variability of the front locations south of Australia, we also used 45 XBT sections occupied between December 1992 and March 1999. These sections have been occupied as a part of the joint Australia–France–USA SURVOSTRAL program (Rintoul et al., 1997, in press(b)). The XBT and CTD sections have nearly the same end-points, but are not coincident along their length: the XBT sections are located some 50–200 km east of SR3 (Fig. 1).

The contours in Fig. 1 indicate the variability of the currents in the region, as reflected in the standard deviation of SSH. The largest variability on SR3 is found between 48° and 53°S, which will correspond
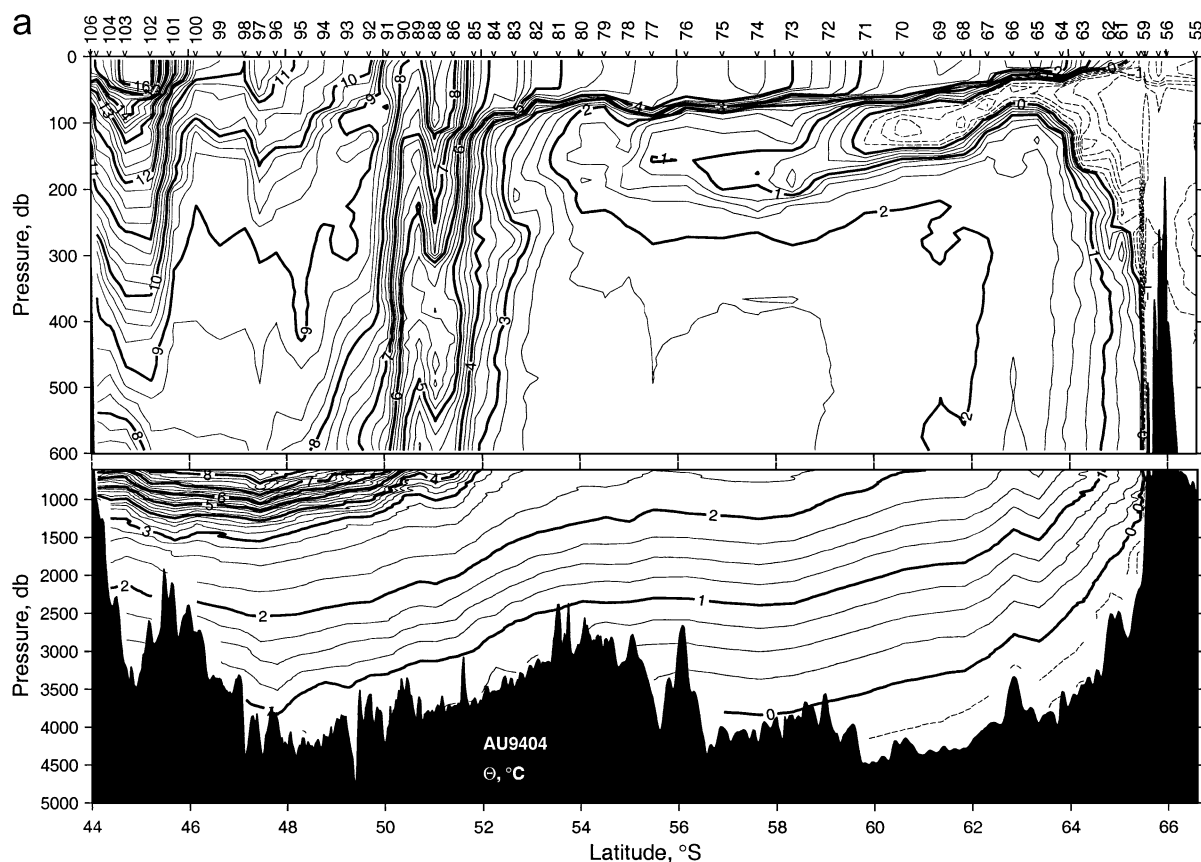

Fig. 2. Property distributions on the January 1995 (au9404) occupation of SR3. (a) Potential temperature (°C), (b) salinity (on the practical salinity scale), (c) neutral density anomaly (kg m^{-3}). Station numbers are indicated at the top of the plot.
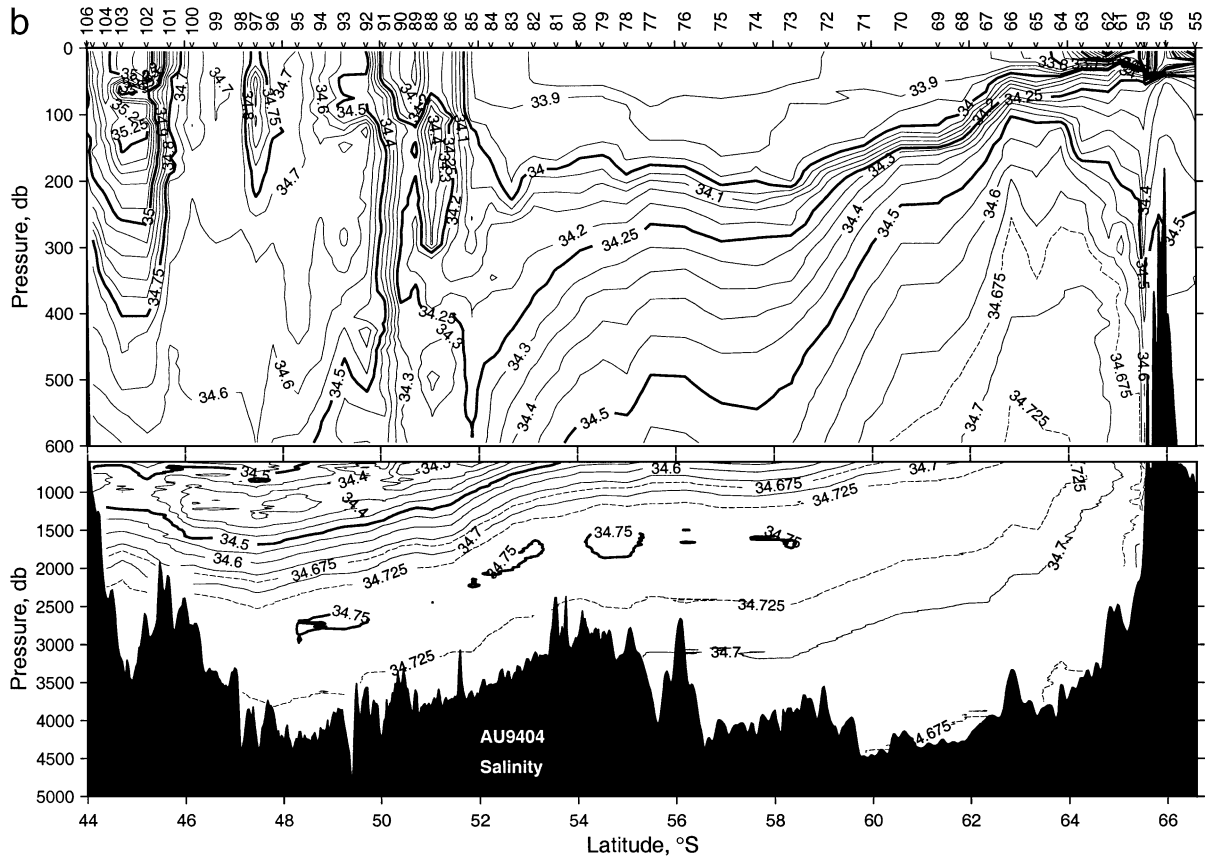
Fig. 2 (*continued*).

to the SAF and PF. These fronts are the strongest and most variable current cores crossing SR3, and they carry most of the transport (Rintoul and Sokolov, 2001). The magnitude of the variability increases downstream (to the east) of SR3, before decreasing in intensity again near 160°E in the vicinity of the Macquarie Ridge.

3. Front characteristics and indicators

In this section, we examine a number of criteria to identify each of the fronts and compare the results to definitions used in previous studies. Oceanic fronts are usually defined by an enhanced lateral (horizontal and/or isopycnal) gradient of some property. In particular, the ACC fronts coincide with large horizontal gradients of density, which are associated with veloc-

ity and transport maxima (Nowlin et al., 1977; Nowlin and Clifford, 1982; Orsi et al., 1995; Belkin and Gordon, 1996). Therefore, we use the distribution of lateral property gradients and transport to identify the Southern Ocean fronts. We then examine whether scalar criteria (e.g. a particular isotherm at a particular depth) exist which coincide with the zones of high gradient. In addition, the current cores associated with Southern Ocean fronts are of finite width, and so it is sometimes useful to distinguish between "axial" values which coincide with the "core" of a front, and criteria which define the northern and southern extent of a front. The latter is particularly important when considering integral quantities, such as the transport carried by a front.

Due to space limitations, it is not possible to show vertical sections of each property at each of the six SR3 sections. We use one of the sections (from
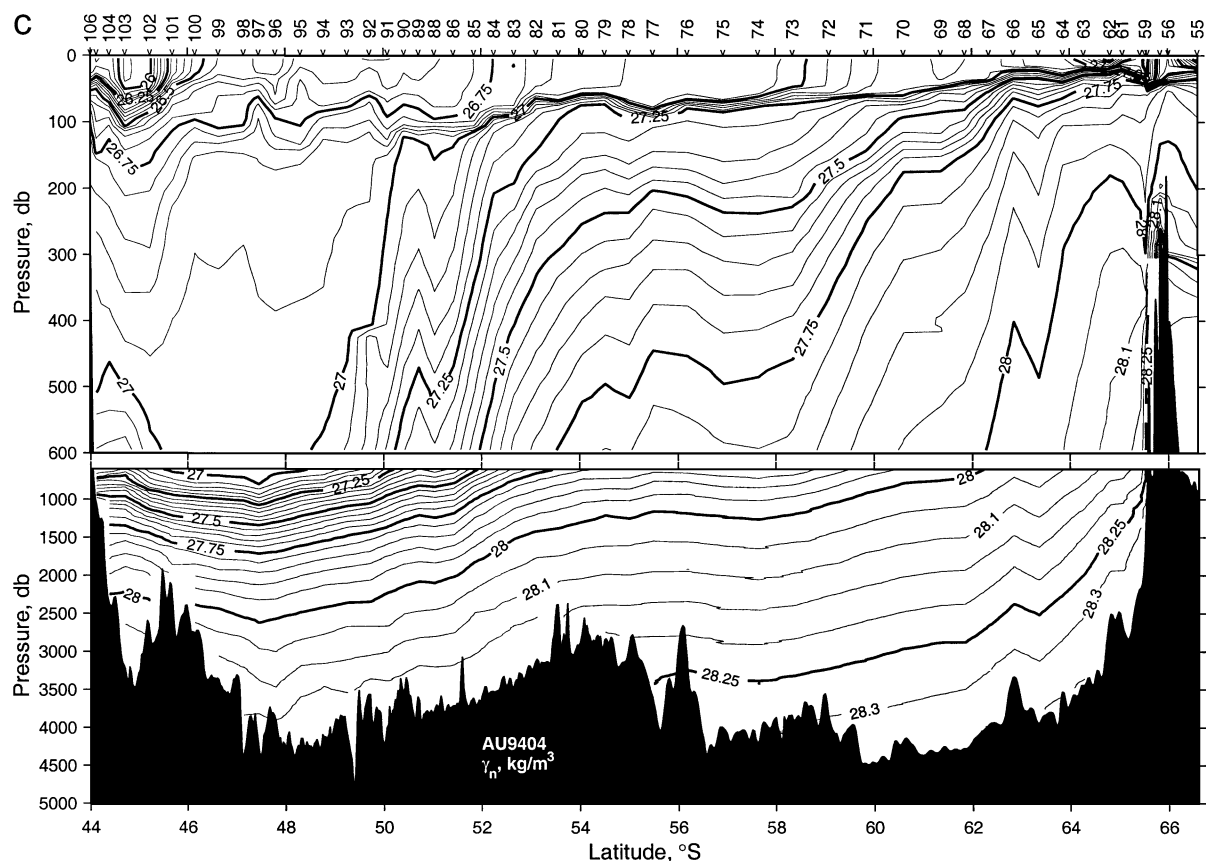
Fig. 2 (*continued*).

January 1995) as an example, and include a summary figure of various frontal indicators for each of the sections. The potential temperature (θ), salinity (S) and density (γ_n) distributions along the SR3 section in January 1995 are shown in Fig. 2. As typically seen in meridional sections across the ACC, the temperature decreases to the south in a series of steps or fronts, separated by zones of weaker meridional gradient. These steps are also associated with changes in salinity (e.g. the shoaling of the salinity maximum layer) and density (e.g. enhanced isopycnal tilt throughout the water column).

Fig. 3 shows the bands of enhanced horizontal gradient more clearly. Fronts are found near 45°S, between 50° and 53°S, between 58° and 60°S, and near 62°, 64°S, and the Antarctic continental margin. Note that the maxima in horizontal gradients in one property do not always coincide with those in another

property: e.g. the horizontal salinity gradient has a maximum near 1000–1500 dbar at 52°S, where the horizontal potential temperature gradient is close to a relative minimum (Fig. 3). As discussed below, different criteria will better define the fronts in different depth or density ranges.

We also found sections of temperature, salinity and oxygen with neutral density as the ordinate to be useful for identifying fronts which separate distinct water masses (e.g. Fig. 4). For example, the STF near 45.6°S is associated with strong along-isopycnal gradients of θ, S, and oxygen for $\gamma_n < 26.9$ kg m^{-3}.

To look in more detail at the fronts, we plotted a large number of properties versus latitude along each section. Fig. 5 shows some examples for the January 1995 section illustrated in Figs. 2 and 3: temperature on various surfaces (along isobars and along the temperature minimum and temperature maximum

layers), horizontal temperature gradient at several depths, transport, and the horizontal gradient of sea surface height. Figs. 6–10 show similar plots for each of the other SR3 sections. From these plots, a list of criteria corresponding to each front was compiled (Tables 2–5). From this analysis, we found that a few simple proxy criteria can be used to identify the fronts consistently. These criteria are summarized in Table 6. Front positions based on these criteria are shown by the shaded bars in each panel of Figs. 5–10. These positions generally coincide with fronts as defined by maxima in horizontal gradient and transport, to within the resolution of the station spacing, as discussed below.

Before considering each of the fronts in turn, we introduce briefly the major water masses found along the section, as Southern Ocean fronts are frequently defined in relation to particular water masses. The Subtropical Lower Water (SLW), characterized by a high salinity core located between the surface and 200 m depth, is found north of about 45°S. The thick uniform layer from 100 to 500 dbar between 46° and 50°S is the Subantarctic Mode Water (SAMW). A salinity minimum below the SAMW thermostad marks the Antarctic Intermediate Water (AAIW). The relatively fresh surface water south of 53°S is the Antarctic Surface Water (AASW). Below the AASW is a temperature minimum (θ_{min}) layer. Winter cooling forms a cold, relatively deep (200 m) mixed layer in winter in this region. Summer warming creates a shallow warm mixed layer above the remnant winter mixed layer water, forming a θ_{min}. The θ_{min} is therefore sometimes called Winter Water. Below the θ_{min} lies a temperature maximum layer, which coincides with the Upper Circumpolar Deep Water (UCDW). The UCDW also corresponds to a nutrient maximum and oxygen minimum (Callahan, 1972). The Lower Circumpolar Deep Water (LCDW) corresponds to the salinity maximum found below the UCDW. Finally, the cold, fresh layer near the bottom on the southern half of the section marks the Antarctic Bottom Water (AABW).

3.1. Subtropical front

The STF separates warm salty subtropical water from fresh cool subantarctic water further south. The STF is associated with strong temperature and sal-

inity gradients in the upper 400 m at 45.6°S in January 1995 (Figs. 2 and 3). The STF coincides with a decrease in temperature at 150 m (θ_{150}) from >12 to <10 °C (bold line, Fig. 5a) and a maximum in the horizontal temperature gradient at this depth (bold line, Fig. 5b). The temperature and salinity gradients of the STF are largely density-compensating (compare Fig. 2a, b to c) and the geostrophic flow associated with the front is weak. The weak, shallow eastward shear of the STF is more than compensated by westward flow at deeper levels (Rintoul and Sokolov, 2001), so the STF does not correspond to a maximum in top-to-bottom transport (Fig. 5c) or in the gradient of SSH ($\nabla\eta$, Fig. 5d).

As can be seen from Figs. 6–10, the STF can be identified in a similar way in each of the repeats of SR3. Table 2 lists characteristic values of temperature, salinity, density and oxygen of the SLW and SAMW that lie to the north and south of the STF, respectively; these characteristics can help identify the STF even if the data lacks sufficient resolution to calculate gradients reliably. The latitude of the front is relatively steady, varying between 44.5° and 45.6°S on the six SR3 sections (Table 2). Only the southern branch of STF is crossed by the SR3 section south of Tasmania. To the east of the section in the southern Tasman Sea, the Subtropical Frontal Zone is broad and consists of several frontal branches, which stretch across the Tasman Sea within the limits identified by Deacon (1937) and Garner (1967). Multiple branches of the STF are also found in the Indian and Atlantic Sectors of the Southern Ocean (Belkin and Gordon, 1996).

A number of criteria have been used to identify the STF (e.g. Table 4 in Belkin and Gordon, 1996). Many of these definitions apply at SR3. In particular, the criteria of Clifford (1983) (axial temperature and salinity at 200-m depth of 10 °C and 34.8, respectively) and Nagata et al. (1988) (axial temperature of 11 °C at 150-m depth) coincide with strong horizontal temperature and salinity gradients south of Tasmania (e.g. Fig. 2).

3.2. Subantarctic Front

The SAF, the strongest front and main jet of the ACC south of Australia, corresponds to the zone of large horizontal gradients between 50° and 53°S at

SR3. In this latitude band, temperature at 200 dbar decreases from north to south by more than 5 °C. The $\gamma_n = 27.25$ surface deepens from 150 m south of the front to almost 1000 m north of the front. The enhanced horizontal gradients of the SAF extend from the sea surface to the sea floor (Figs. 2 and 3).

A variety of features have been used to define the SAF: an axial temperature or salinity at a particular depth, a maximum horizontal temperature gradient, the northward descent of the prominent salinity minimum associated with AAIW, or the presence of a thick thermostad (the SAMW) immediately to the north (see Table 2 in Belkin and Gordon, 1996 for a summary). Most previous studies using such criteria have identified a single branch of the SAF. On SR3, we consistently find two branches of the SAF (Belkin and Gordon, 1996 note that several earlier sections also showed a "double" SAF in this

sector). Each of the branches corresponds to maxima in horizontal gradients of temperature, salinity and density, although the depth of the gradient maxima differs between properties and between the two fronts. The northern SAF coincides with a decrease in θ from >8 to <6 °C at 300 to 400 dbar and maxima in $\nabla\theta(300-400 \text{ dbar})$ and $\nabla\eta$; the southern SAF coincides with a decrease in θ from >6 to <4 °C at 300 to 400 dbar and maxima in the horizontal gradients of θ and η (Figs. 5–10, Table 3). Each of the two branches coincides with enhanced along-isopycnal gradients of θ, S, and oxygen for $\gamma_n < 27.5$ kg m^{-3} (Fig. 4). The northern branch is usually located between 50° and 51°S, while the southern branch is found between 52° and 53°S. Fig. 2 illustrates the "split" nature of the SAF. In this particular example, the isotherms reverse slope between the two branches of the SAF, consistent
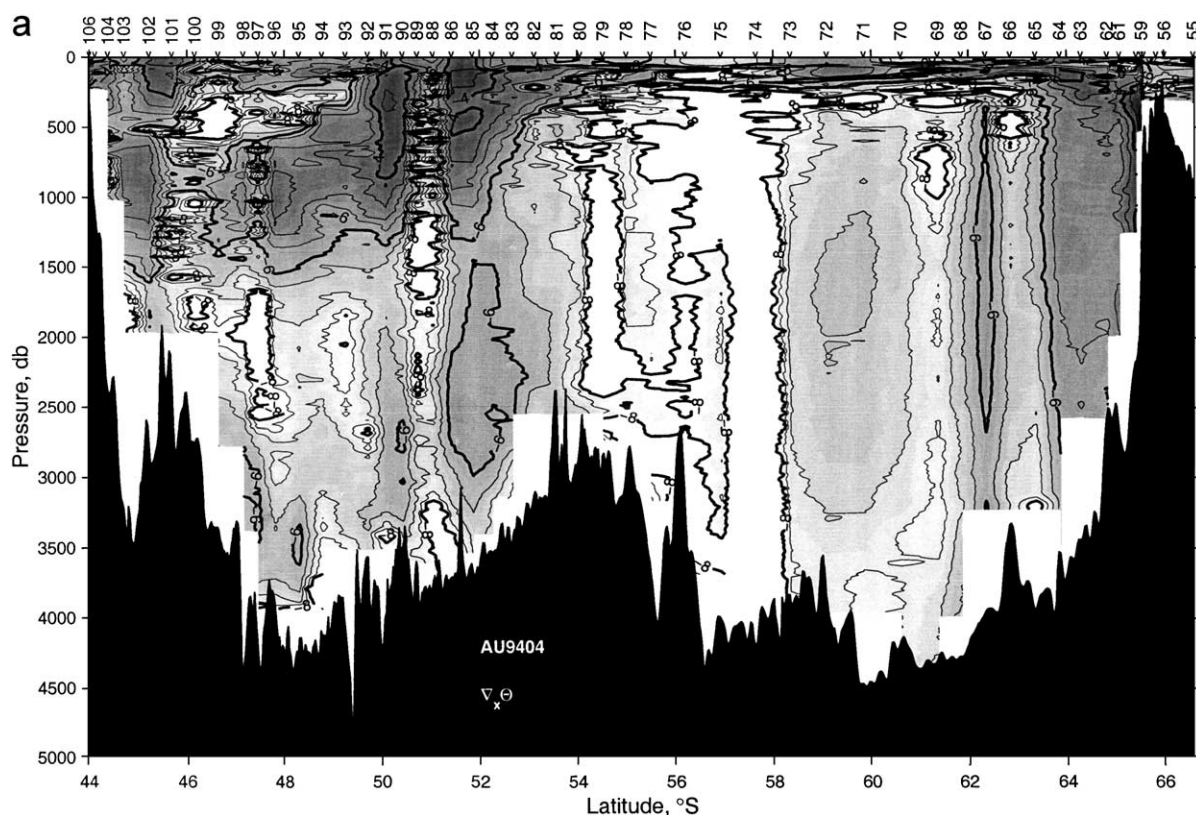

Fig. 3. Horizontal gradients of (a) potential temperature and (b) salinity on the January 1995 SR3 section shown in Fig. 2, on a logarithmic scale. Gradients are evaluated from station pair differences.
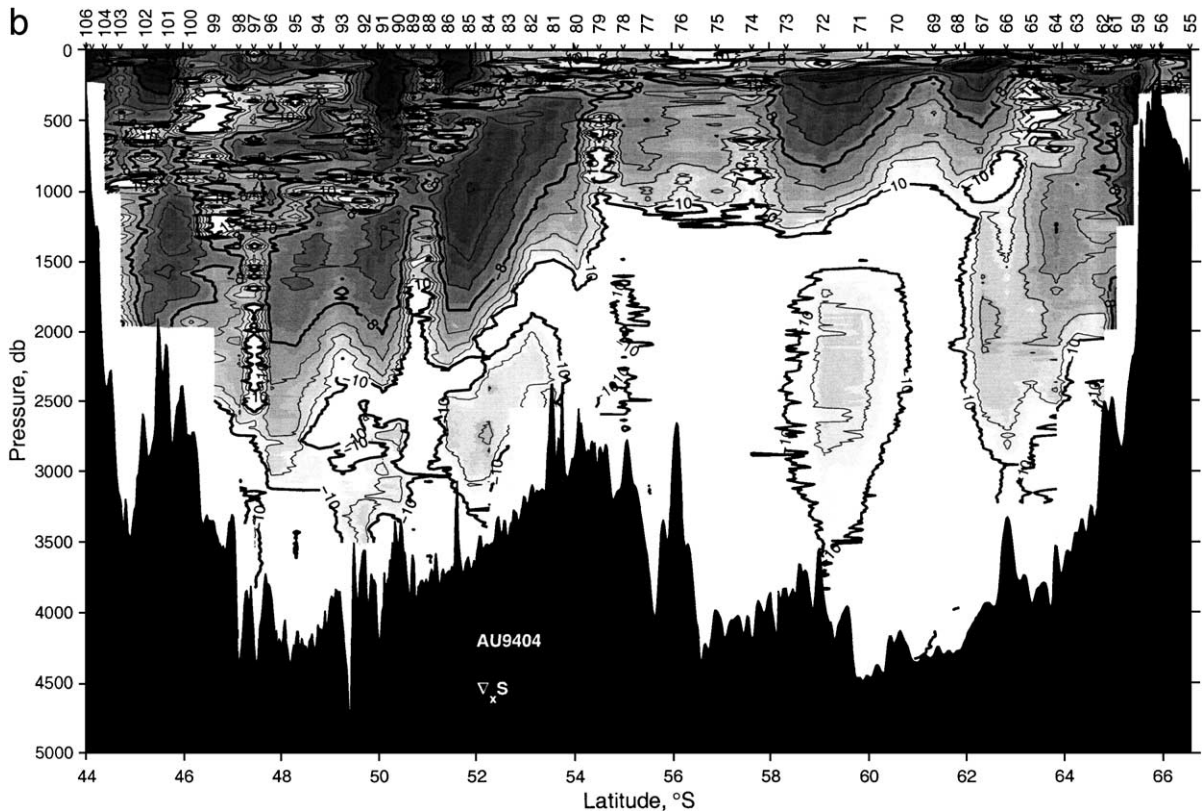
Fig. 3 (*continued*).

with a meander of the front. (This interpretation is confirmed by maps of sea surface height, see below.) Figs. 6–10c show that each of the SR3 sections has a double peak in eastward transport in the SAF. In September 1996, a weaker third transport maximum occurs between the two main branches of the SAF, associated with enhanced lateral density gradients (Fig. 11).

The contribution of the horizontal gradients of temperature and salinity to the horizontal gradient of density differs across the two branches of the SAF. Temperature and salinity both decrease to the south across the northern branch of the SAF above the depth of the salinity minimum layer. The temperature and salinity gradients therefore tend to compensate each other in their effect on density; this compensation is nearly complete in the mixed layer (Figs. 2c and 11; see also Rintoul and Trull, 2001). Below the depth of the salinity minimum, temperature

decreases and salinity increases to the south, so the two fields both contribute to the southward increase in density.

Salinity changes across the southern branch of the SAF are weak in the upper 600 m, so temperature makes the dominant contribution to density changes there. At greater depths, the southward increase in salinity is associated with the shoaling of UCDW across the SAF (Fig. 2b). The UCDW is found between 1500- and 2500-m depth north of the SAF, and shoals to depths of 400 to 1000 m south of the SAF. The temperature of the UCDW is relatively uniform, so in this depth range, salinity makes the dominant contribution to the poleward increase in density (Fig. 3). At greater depths, in the salinity maximum layer of the Lower Circumpolar Deep Water (LCDW), changes in temperature again make the dominant contribution to changes in density.

3.3. Polar Front

The PF marks the northern limit of the Antarctic Zone (Gordon et al., 1977) and is commonly defined by the northernmost extent of the subsurface temperature minimum (θ_{min}) cooler than 2 °C, where the θ_{min} ends or dips abruptly below 200 m (see Belkin and Gordon, 1996 for a summary). Analysis of historical hydrographic measurements of the PF shows that the along-front variability of the surface temperature is small (Buinitsky, 1973), and the PF is well approximated by the 2 °C isotherm in the subsurface (θ_{min}) layer almost everywhere in the Southern Ocean (Botnikov, 1963).

The PF at SR3 is clearly composed of two branches, as noted earlier by Rintoul and Bullister (1999) and Rintoul and Sokolov (2001). The north-ern limit of θ_{min} water cooler than 2 °C, the most commonly used definition of the PF, generally coincides with a deep-reaching front near 53.6°S (e.g. Figs. 2–5). A second deep-reaching front between 58 and 60°S is also found on every occupation of SR3 (e.g. (Figs. 2, 3 and 11)). The front generally coincides with the southernmost extent of water warmer than 2.2 C in the θ_{max} layer. Rintoul and Bullister (1999) called the latter front the southern branch of the PF, because it corresponded with PF definitions used by some authors at other locations. For example, the south-ern branch tends to coincide with an increase in depth of the θ_{min} (Gordon, 1967, 1971), the north-ern limit of the 0 to 1 °C isotherms in the θ_{min} (Burling, 1961; Nowlin et al., 1977; Nagata et al., 1988), and an enhanced temperature gradient along
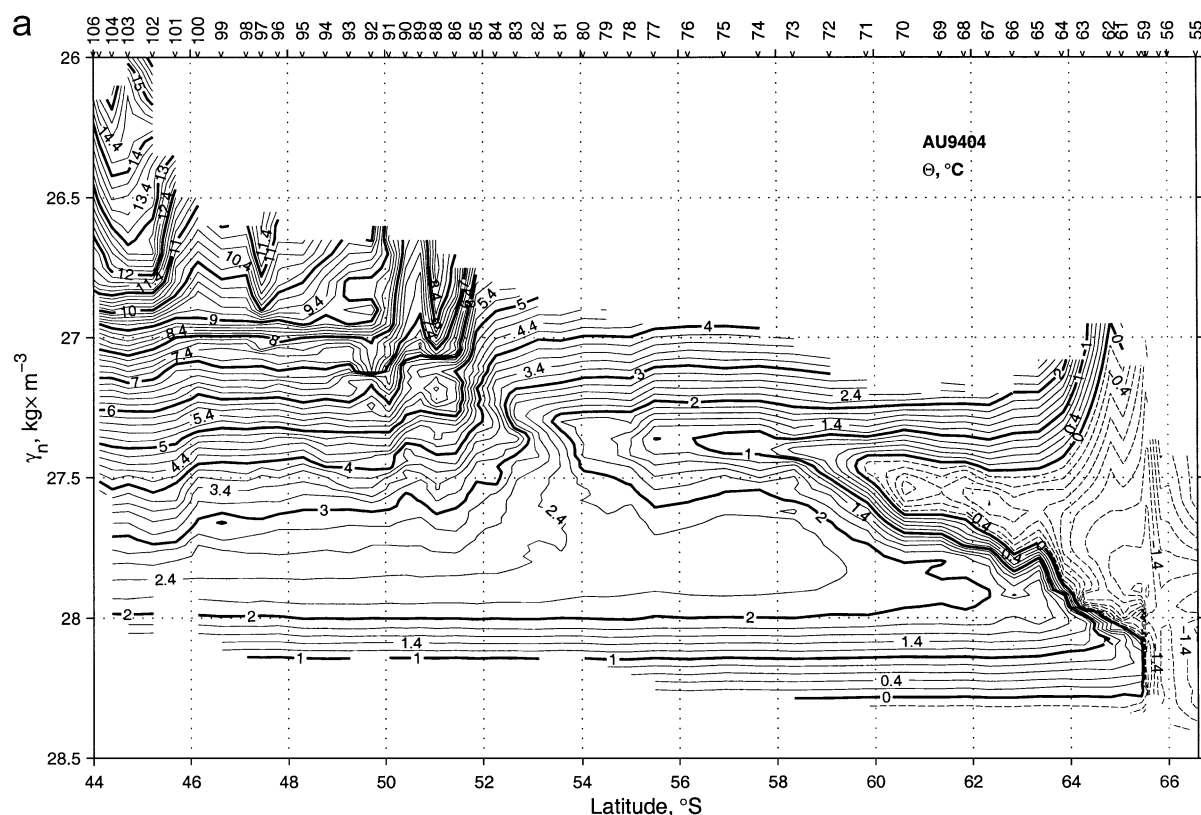

Fig. 4. Distribution of (a) potential temperature (°C) and (b) oxygen (μmol kg^{-1}) along the January 1995 occupation of SR3, with neutral density as the ordinate.
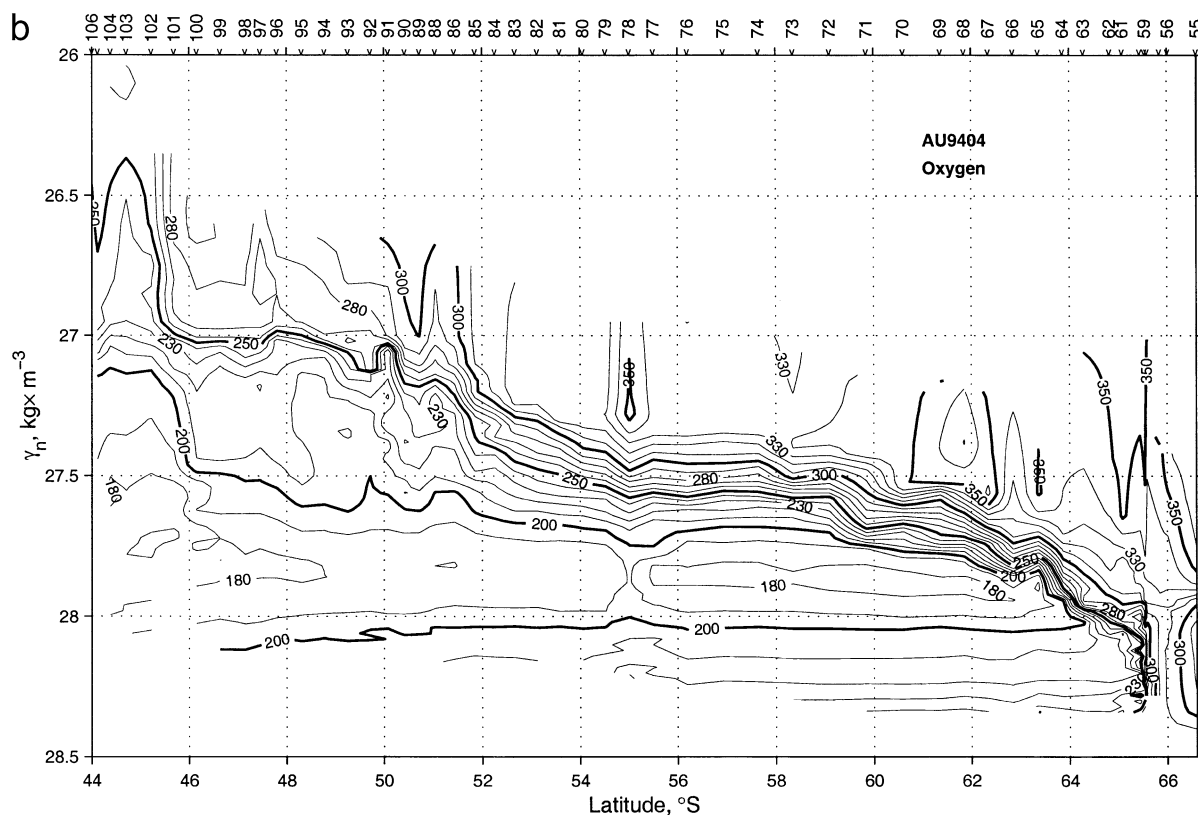
Fig. 4 (*continued*).

the θ_{min} (Figs. 5–10e). Both branches of the PF coincide with transport maxima (Figs. 5–10c).

A number of other features coincide with the PF and help to distinguish between the northern and southern branches, as summarized in Table 4. The 34.5 isohaline shoals to the south by about 200 or 300 dbar across each branch of the PF (e.g. Fig. 2b). The depth of the 34.0 isohaline does not change across the northern PF, but decreases in depth across the southern PF. As a result of these changes, the layer bounded by these two isohalines thins to the south across each branch of the PF. A similar pattern is evident in the $\gamma_n = 27.25$ and $\gamma_n = 27.75$ neutral surfaces and the layer between them (Fig. 2c). Both branches of the PF correspond to maxima in the along-isopycnal gradients of θ, S, and oxygen, although the maximum gradients occur at slightly greater density across the southern PF

(Fig. 5, Table 4). The location of both branches of the PF is very steady in time (Table 4). Between the two branches of the PF, the isopleths are flat, indicating little flow across the section (Fig. 2). This is consistent with the mean dynamic topography (e.g. Olbers et al., 1992), which shows that the flow is more or less along the section in this latitude band, as discussed in more detail below.

Two branches of the PF have also been found at other longitudes (e.g. Drake Passage (Sievers and Nowlin, 1984), the southern Indian Ocean (Sparrow et al., 1996), and the south Pacific (Moore et al., 1999; Read et al., 1995)). The northern branch is often called the "subsurface expression" of the PF, because it is identified by a subsurface temperature criterion (the northern limit of the θ_{min}), while the southern branch often corresponds to an SST gradient and so is called the "surface expression" of the PF. This nomenclature

may give the misleading impression that the PF consists of a single front whose "surface" and "subsurface" expressions are displaced from each other.

We prefer to make it clear that both features extend throughout the water column by referring to the northern and southern branches of the PF.
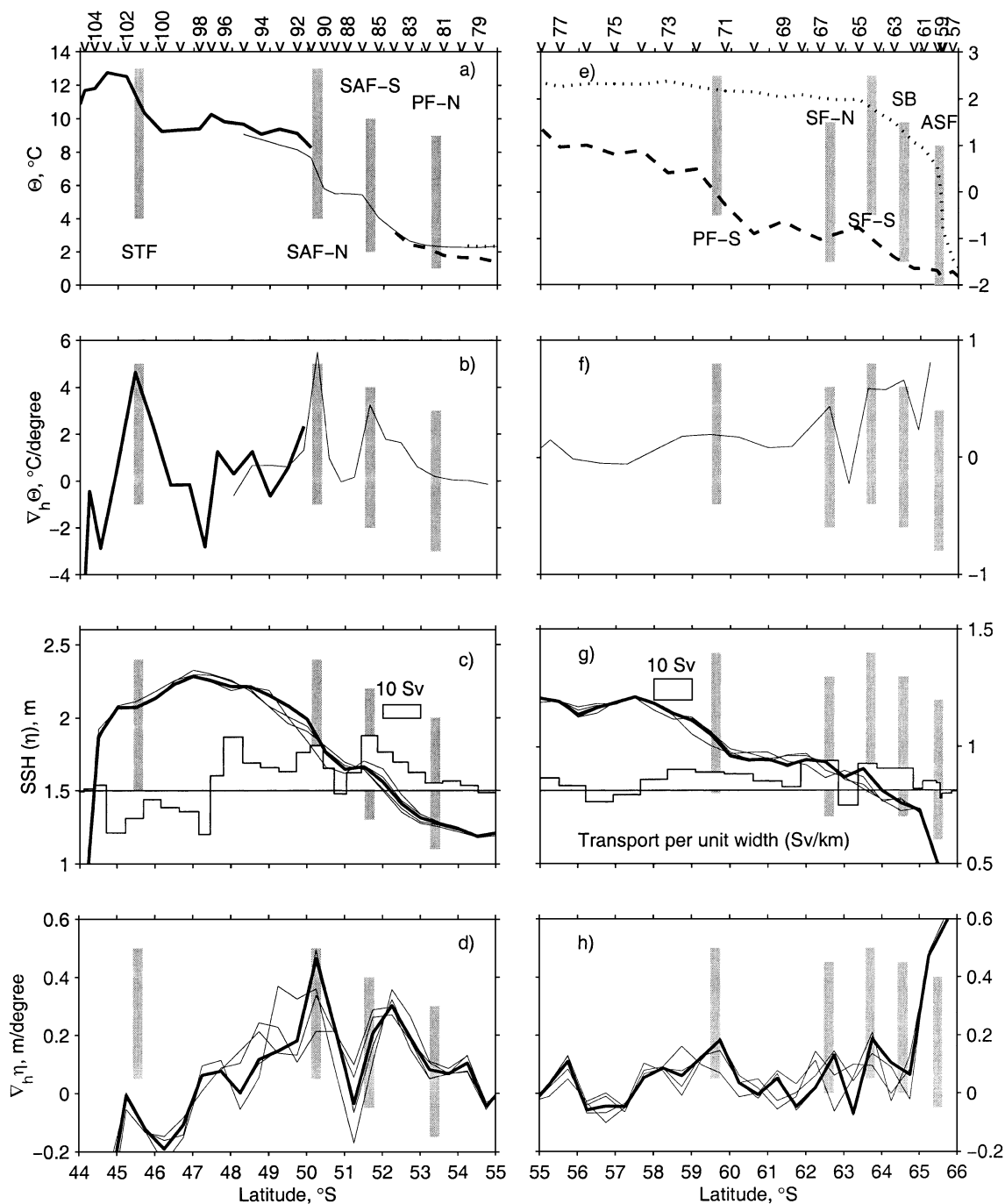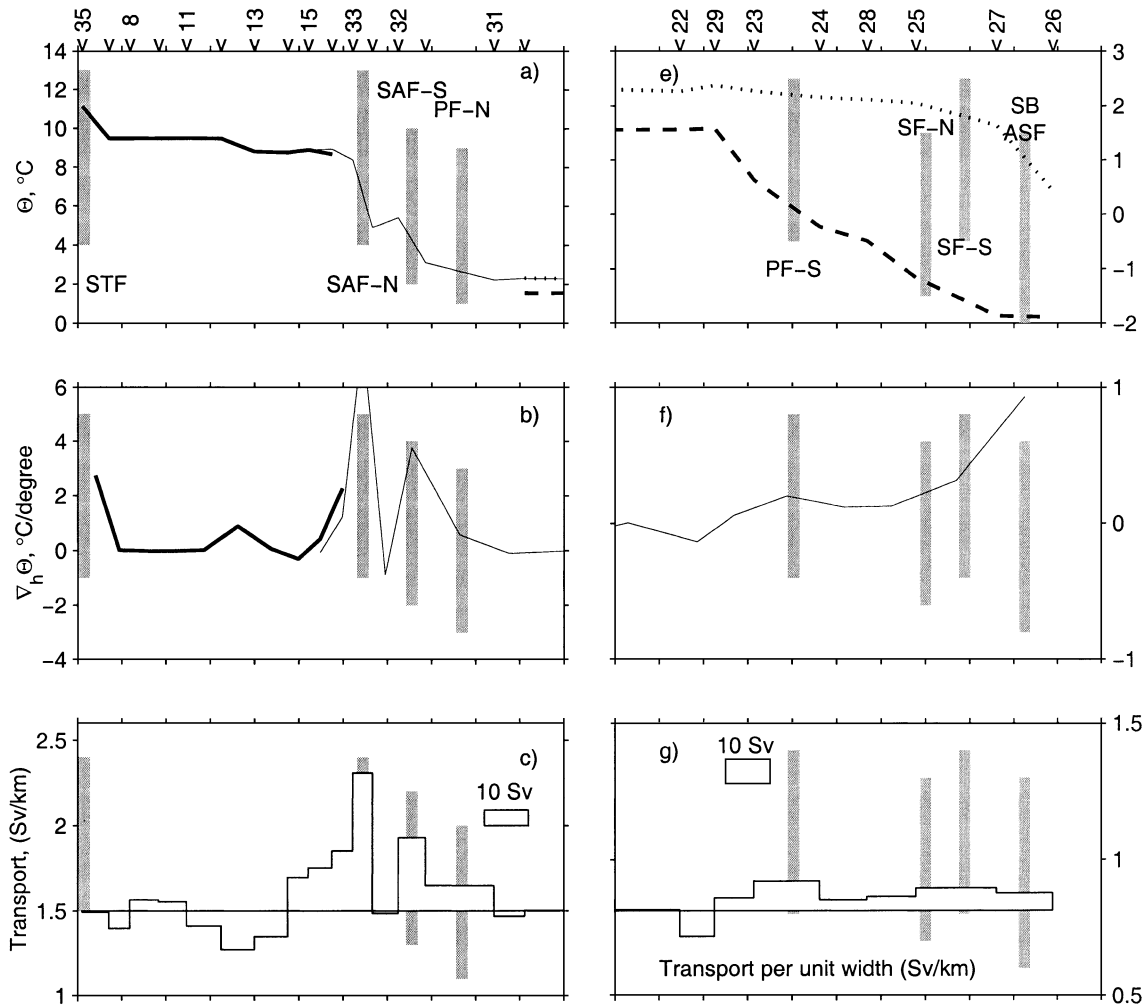
Fig. 6. Same as Fig. 5, for the October 1991 occupation of SR3.

3.4. Southern fronts

Orsi et al. (1995) identified two additional ACC fronts south of the PF—the southern ACC front

(SACCF) and the southern boundary of the ACC (SB). The SACCF and SB are generally distinct features, but may be adjacent to each other at some locations. Orsi et al., 1995 found the SACCF usually

Fig. 5. Correspondence between various indicators and front positions on the January 1995 SR3 section shown in Fig. 2. (a) Potential temperature at 150 dbar (bold line), at 400 dbar (thin line), at the temperature minimum (bold dashed line), and at temperature maximum (dotted line). (b) Horizontal potential temperature gradient at 150 dbar (bold line) and 400 dbar (thin line). (c) Sea surface height (m) mapped to the time and location of the SR3 stations (thin line) and transport per unit width from Rintoul and Sokolov (2001) (open bars; scale bar = 10 Sv). (d) Horizontal gradient of sea surface height (thin line). Panels (e–h) are as in panels (a–d), for the southern half of the section except in panel (f) horizontal potential temperature gradient at 1500 dbar. Front positions corresponding to the front indicators listed in Table 6 are marked by shaded bars (STF, Subtropical Front; SAF, Subantarctic Front; PF, Polar Front; SF, southern ACC front; SB, southern boundary of the ACC; ASF, Antarctic Slope Front. Northern and southern branches of each front, where applicable, are indicated by -N and -S (e.g. SAF-S is the southern branch of the SAF). Station numbers are indicated at the top of the plot.
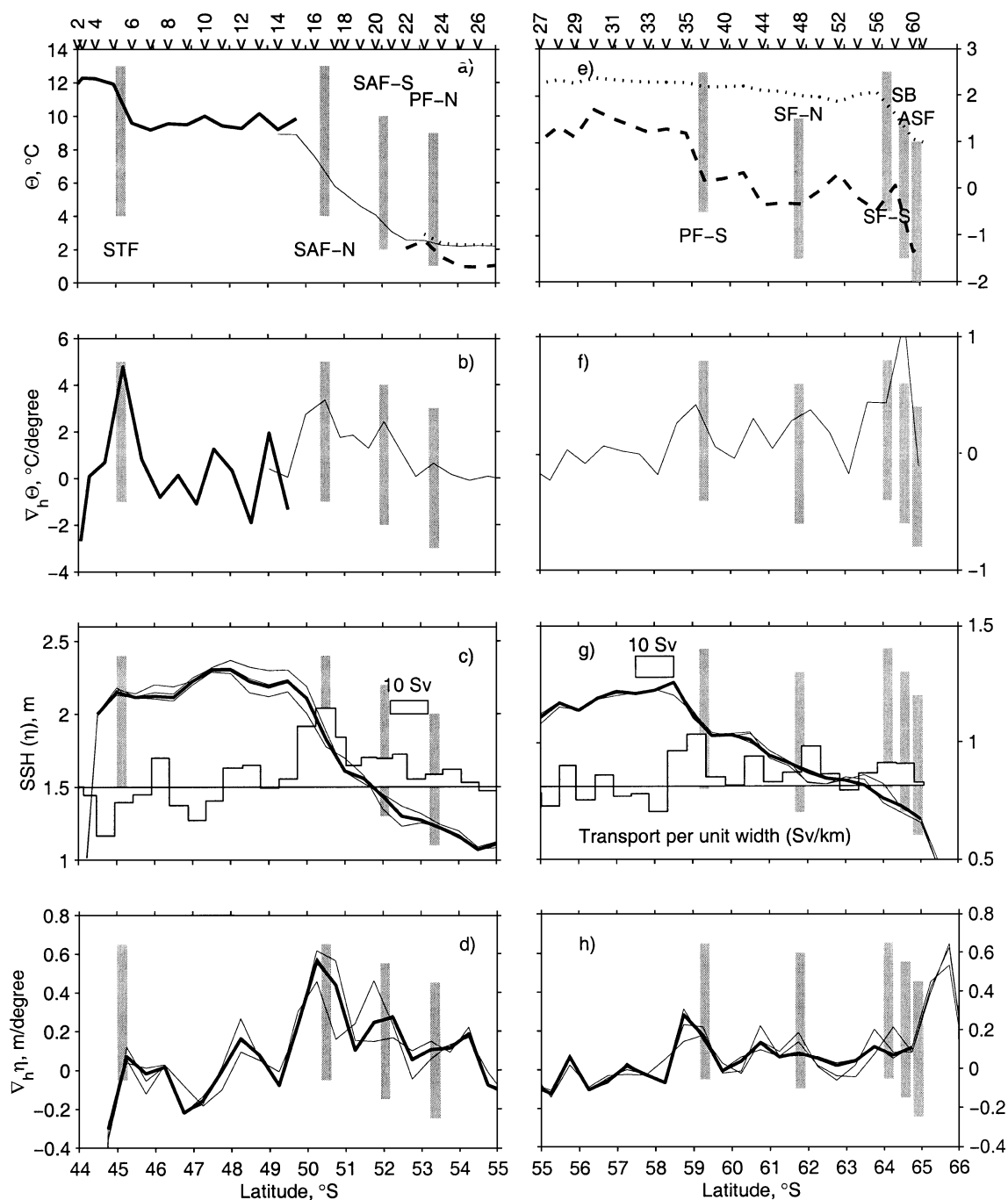
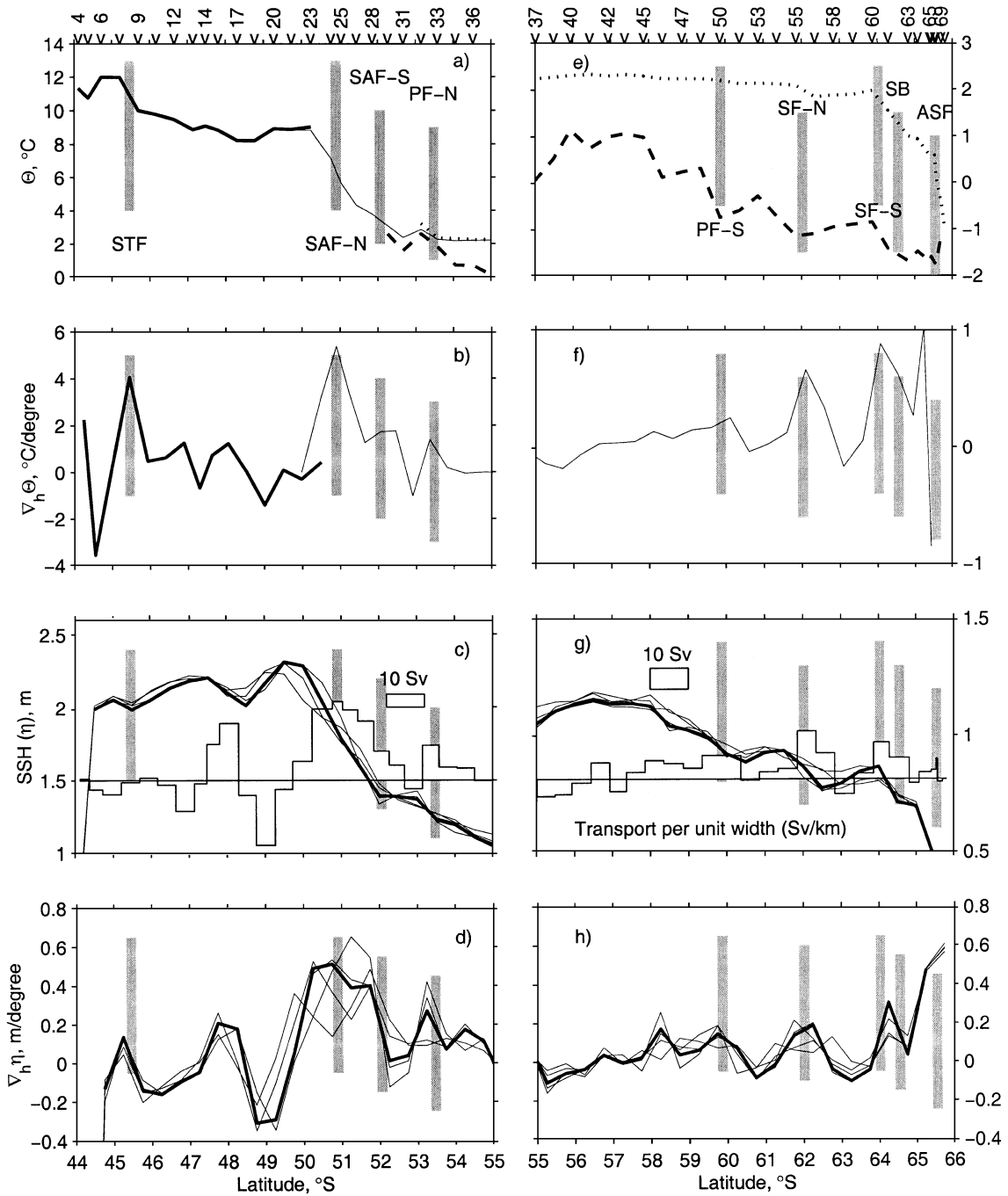Fig. 7. Same as Fig. 5, for the March 1993 occupation of SR3.

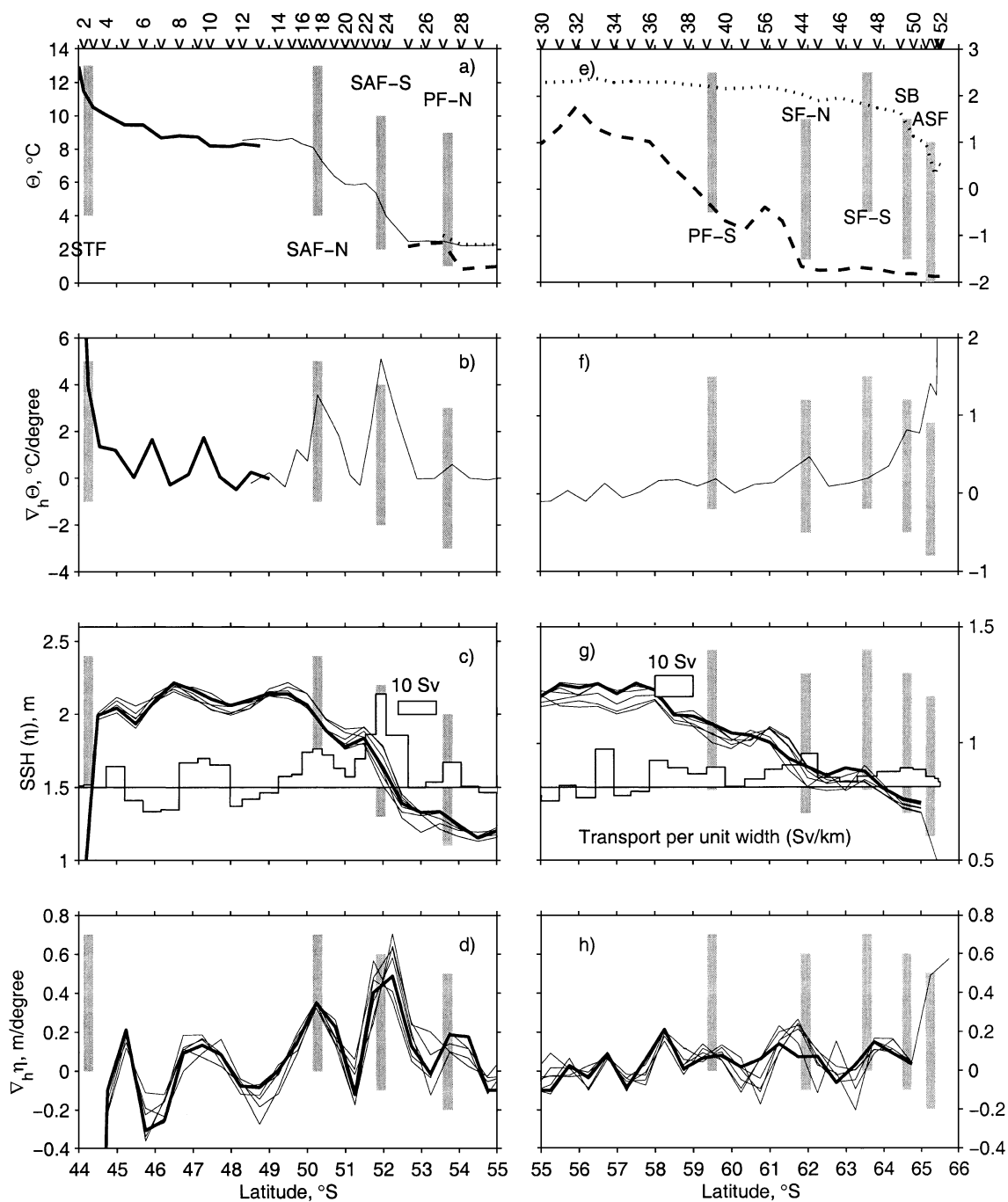Fig. 8. Same as Fig. 5, for the January 1994 occupation of SR3.

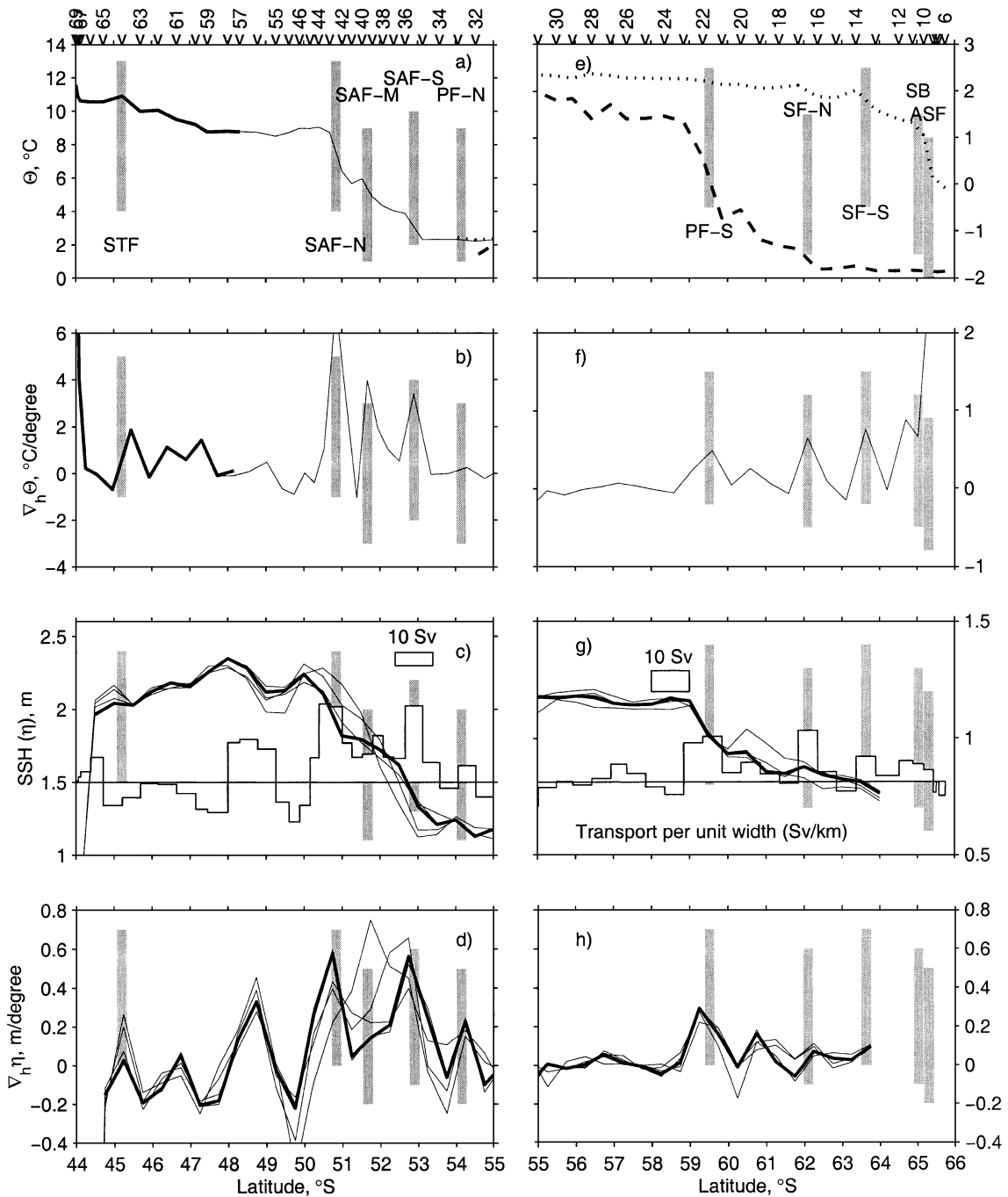Fig. 9. Same as Fig. 5, for the July 1995 occupation of SR3.

Fig. 10. Same as Fig. 5, for the September 1996 occupation of SR3.

Table 2
T, S, γ_n and oxygen ranges of STF at WOCE SR3

Cruise	Position	Temperature		Salinity		γ_n		Oxygen	
		South[a]	North	South	North	South	North	South	North
au9101	44.5°S	9.25	>11	34.70	>35	26.95	26.85	275	...
au9309	45.2°S	9.25	15.00	34.65	35.25	26.90	26.80	270	210–230
au9407	45.6°S	9.25	13.75	34.65	35.25	26.90	26.85	280	240–260
au9404	45.6°S	9.25	16.25	34.65	35.30	26.95	26.85	275	240
au9501	44.7°S	8.75	13.00	34.60	35.25	26.95	26.85	270	260
au9601	45.6°S	8.75	11.50	34.60	35.05	26.95	26.80	270	265

[a] Typical values of T, S, γ_n and oxygen for the SAMW (south of the front) and the SLW (north of the front) are given. The depth range of the STF is limited by the upper 500 m.

coincided with the southern-most extent of water >1.8 °C in the θ_{max} of the UCDW, and they noted that it is the only Southern Ocean front that does not separate distinct surface water masses. The SB represents the poleward limit of the circumpolar circulation, which they found to coincide with the poleward limit of low-oxygen UCDW.

On SR3 several closely spaced, distinct fronts are found south of the southern PF, in almost the same locations on each repeat of the section (Table 5). A front between 62° and 63°S corresponds with the southern limit of θ_{max} water warmer than 2 °C and to maxima in $\nabla\theta$, $\nabla\eta$, and transport (Figs. 5–10; Table 5). A second front at 64°S corresponds with the southern limit of θ_{max} water warmer than 1.8 °C

(Figs. 5–10; Table 5), the criterion used by Orsi et al. (1995) to identify the SACCF. Therefore, it seems most appropriate to refer to these two features, which are distinct in every occupation of SR3, as the northern and southern branch of the SACCF. The latitude of each branch of the SACCF is very steady in time at SR3 (Table 5), varying by less than ± 0.5° about its mean latitude.

The SB is best defined by the southern limit of the oxygen minimum associated with UCDW (Fig. 4c). On SR3, this feature is coincident with the southern limit of θ_{max} water warmer than 1.5 °C, and with weak maxima in $\nabla\theta$ and transport (Figs. 5–10e–h). The SB is located between 64° and 65°S, about 1° south of the southern branch of the SACCF (Table 5).

Table 3
θ, S, and γ_n ranges at 300–400 m depth across the SAF at WOCE SR3

Cruise	Branch	Position, °S	θ, °C	Salinity	γ_n, kg × m^{-3}	η^a, m
au9101	northern	50.4	6–8	34.2–34.6	26.95–27.15	...
	southern	∼ 52	3–6	–	27.20–27.60	...
au9309	northern	50.5	6–8	34.2–34.6	26.95–27.25	$\frac{1.6\rightarrow2.1}{1.8}$
	southern	52	3–4	–	27.30–27.50	$\frac{1.3\rightarrow1.6}{1.45}$
au9407	northern	50.9	5–8	34.1–34.5	26.95–27.25	$\frac{1.6\rightarrow2.1}{1.8}$
	southern	52.1	3–4	–	27.35–27.50	$\frac{1.4\rightarrow1.6}{1.4}$
au9404	northern	50.2	6–8	34.2–34.6	27.00–27.10	$\frac{1.7\rightarrow2.1}{1.9}$
	southern	51.7	3–6	–	27.20–27.45	$\frac{1.4\rightarrow1.7}{1.6}$
au9501	northern	50.3	7–8	34.3–34.5	26.95–27.05	$\frac{1.8\rightarrow2.1}{1.95}$
	southern	52.0	3–6	34.2–34.4	27.15–27.45	$\frac{1.4\rightarrow1.8}{1.6}$
au9601	northern	50.9	7–9	34.3–34.6	26.95–27.10	$\frac{1.8\rightarrow2.1}{1.9}$
	middle	51.7	5–6	34.15–34.25	27.10–27.20	$\frac{1.6\rightarrow1.8}{1.75}$
	southern	52.9	3–4	–	27.40–27.60	$\frac{1.3\rightarrow1.6}{1.35}$

[a] η—SSH. Mean dynamic height (relative to 2500 dbar) estimated from the six repeats of SR3 is added to SSH anomalies measured by satellite altimetry. Triple values for η correspond to southern limit, northern limit and axis of the front.

Table 4
Indicators of the PF at WOCE SR3

Cruise	au9101	au9309	au9407	au9404	au9501	au9601
NPF						
Position[a], °S	$\frac{53.4 \to 51.9}{53.0}$	$\frac{54.1 \to 53.1}{53.6}$	$\frac{54.1 \to 53.1}{53.6}$	$\frac{54.1 \to 53.1}{53.6}$	$\frac{54.1 \to 53.6}{53.8}$	$\frac{54.5 \to 54.1}{54.3}$
p[b] at $S=34.5$, dbar	$400 \to 825$	$480 \to 660$	$510 \to 740$	$560 \to 680$	$480 \to 640$	$430 \to 540$
p at $S=34.0$, dbar	$150 \to 150$	$170 \to 170$	$200 \to 220$	$160 \to 180$	$180 \to 180$	$160 \to 160$
h_S[c], dbar	$250 \to 675$	$310 \to 490$	$310 \to 520$	$400 \to 500$	$300 \to 460$	$270 \to 380$
p at $\gamma_n=27.75$, dbar	$350 \to 800$	$430 \to 630$	$460 \to 740$	$520 \to 660$	$430 \to 620$	$380 \to 510$
p at $\gamma_n=27.25$, dbar	$100 \to 200$	$80 \to 150$	$100 \to 180$	$80 \to 140$	$140 \to 160$	$130 \to 130$
h_{γ_n}[d], dbar	$250 \to 600$	$350 \to 480$	$360 \to 560$	$440 \to 520$	$290 \to 460$	$150 \to 380$
θ in θ_{min} layer, °C	$\frac{1.2 \to 3.0}{2.0}$	$\frac{1.0 \to 2.5}{2.0}$	$\frac{0.2 \to 2.5}{2.0}$	$\frac{1.8 \to 2.5}{2.0}$	$\frac{1.0 \to 2.5}{2.0}$	$\frac{1.4 \to 2.0}{2.0}$
θ in θ_{max} layer, °C	2.25	2.30	2.30	2.40	2.40	2.30
γ_n at max $(\nabla_n\theta)$[e]	$\frac{27.3 \to 27.7}{27.4}$	$\frac{26.9 \to 27.7}{27.4}$	$\frac{27.3 \to 27.8}{27.5}$	$\frac{27.3 \to 27.6}{27.4}$	$\frac{27.3 \to 27.7}{27.4}$	$\frac{27.25 \to 27.7}{27.4}$
η_{SR3}[f], m	...	$\frac{1.15 \to 1.26}{1.21}$	$\frac{1.19 \to 1.33}{1.23}$	$\frac{1.23 \to 1.30}{1.27}$	$\frac{1.23 \to 1.32}{1.27}$	$\frac{1.15 \to 1.22}{1.18}$
η_{Olbers}[g], m	...	$\frac{1.20 \to 1.32}{1.26}$	$\frac{1.25 \to 1.41}{1.26}$	$\frac{1.29 \to 1.33}{1.31}$	$\frac{1.29 \to 1.39}{1.34}$	$\frac{1.25 \to 1.29}{1.27}$
SPF						
Position, °S	$\frac{59.6 \to 58.1}{59.0}$	$\frac{59.3 \to 58.3}{58.9}$	$\frac{60.4 \to 59.4}{59.9}$	$\frac{60.6 \to 58.4}{59.8}$	$\frac{59.8 \to 57.9}{59.4}$	$\frac{59.9 \to 58.8}{59.4}$
p at $S=34.5$, dbar	$280 \to 520$	$320 \to 580$	$220 \to 370$	$240 \to 500$	$290 \to 560$	$275 \to 550$
p at $S=34.0$, dbar	$120 \to 180$	$120 \to 220$	$120 \to 150$	$120 \to 210$	$150 \to 220$	$120 \to 190$
h_S, dbar	$160 \to 340$	$200 \to 360$	$100 \to 220$	$120 \to 290$	$140 \to 340$	$155 \to 360$
p at $\gamma_n=27.75$, dbar	$220 \to 470$	$250 \to 550$	$160 \to 310$	$175 \to 460$	$230 \to 500$	$200 \to 500$
p at $\gamma_n=27.25$, dbar	$-$	$80 \to 130$	$- \to 40$	$60 \to 70$	$-$	$- \to 150$
h_{γ_n}, dbar	$220 \to 470$	$170 \to 420$	$160 \to 270$	$115 \to 390$	$230 \to 500$	$200 \to 350$
θ in θ_{min} layer, °C	$\frac{-0.25 \to 1.5}{1.0}$	$\frac{0.2 \to 1.5}{1.0}$	$\frac{-0.5 \to 0.25}{0}$	$\frac{-0.8 \to 0.5}{0}$	$\frac{-0.5 \to 1.0}{0}$	$\frac{-0.5 \to 1.5}{0.5}$
$p_{\theta_{min}}$[h], dbar	$100 \to 140$	$120 \to 170$	$125 \to 150$	$110 \to 180$	$120 \to 150$	$100 \to 170$
θ in θ_{max} layer, °C	2.20	2.20	2.20	2.20	2.20	2.20
γ_n at max $(\nabla_n\theta)$	$\frac{27.4 \to 27.75}{27.5}$	$\frac{27.4 \to 27.75}{27.5}$	$\frac{27.4 \to 27.8}{27.6}$	$\frac{27.3 \to 27.8}{27.6}$	$\frac{27.4 \to 27.8}{27.55}$	$\frac{27.4 \to 27.75}{27.55}$
η_{SR3}, m	...	$\frac{1.05 \to 1.25}{1.16}$	$\frac{0.89 \to 1.00}{0.94}$	$\frac{0.94 \to 1.16}{0.99}$	$\frac{1.06 \to 1.24}{1.09}$	$\frac{0.96 \to 1.16}{1.06}$
η_{Olbers}, m	...	$\frac{1.11 \to 1.25}{1.21}$	$\frac{0.90 \to 1.06}{1.00}$	$\frac{0.97 \to 1.19}{1.04}$	$\frac{1.10 \to 1.30}{1.16}$	$\frac{1.00 \to 1.23}{1.12}$

[a] Three values for position, θ_{min} and SSH (η) correspond to southern limit, northern limit, and axis of the front.

[b] Two values for pressure (p) and thickness (h) correspond to southern and northern extent of the front.

[c] Thickness of salinity layer between $S=34.5$ and $S=34.0$.

[d] Thickness of density layer between $\gamma_n=27.75$ and $\gamma_n=27.25$.

[e] Upper and low limits, and at max $(\nabla_n\theta)$.

[f] Mean dynamic height (relative to 2500 dbar) estimated from the six repeats of SR3 is added to the SSH anomalies measured by satellite.

[g] Olbers et al. (1992) mean dynamic height (relative to 2500 dbar) is added to the SSH anomalies.

[h] Pressure at the core level of θ_{min} layer.

On some occupations of SR3, the enhanced property gradients associated with the SACCF and the SB are merged. However, dense sampling at the southern end of SR3 (station spacing less than 30 km) generally makes it possible to distinguish the fronts. Property plots on γ_n surfaces show that for these fronts, the maximum θ gradients occur in different density ranges: for the SACCF, $\nabla_n\theta$ is a maximum at $\gamma_n=27.75-27.90$, and for the SB, the maximum $\nabla_n\theta$ is observed at the core level of the UCDW ($\gamma_n=27.90-28.10$).

The southernmost front observed on the SR3 section is the Antarctic Slope Front, which sepa-rates cold and fresh shelf water from warmer and saltier water offshore. On every occasion, except the October 1991 section, which did not extend far enough to the south, the ASF was located at about 65°S. The ASF coincides with an abrupt deepening towards the south of the 34.5 isohaline, from depths of 100–150 m to depths of 250–400 m (Fig. 2). A similar downward slope is also apparent in temperature (e.g. the 0 °C isotherm; Table 5) and oxygen distributions.

Each of the southern fronts corresponds to en-hanced gradients of θ, S and oxygen along isopycnals

Table 5
Indicators of the southern fronts at WOCE SR3

Cruise	au9101	au9309	au9407	au9404	au9501	au9601
Northern SACCF						
Position, °S	$\frac{62.5\to61.3}{61.8}$	$\frac{62.4\to61.3}{61.8}$	$\frac{62.8\to61.3}{61.9}$	$\frac{62.8\to61.9}{62.3}$	$\frac{62.3\to61.3}{61.8}$	$\frac{62.4\to61.8}{62.1}$
p at $S = 34.5$, dbar	$160 \to 230$	$120 \to 220$	$120 \to 240$	$100 \to 210$	$160 \to 220$	$100 \to 220$
p at $S = 34.0$, dbar	$50 \to 100$	$30 \to 90$	$60 \to 120$	$40 \to 100$	$- \to 100$	$- \to 100$
h_S, dbar	$110 \to 130$	$90 \to 130$	$60 \to 120$	$60 \to 110$	$160 \to 120$	$100 \to 120$
p at $\gamma_n = 27.75$, dbar	$110 \to 150$	$80 \to 160$	$80 \to 180$	$60 \to 150$	$- \to 130$	$80 \to 160$
p at $\gamma_n = 27.25$, dbar	$-$	$-$	$-$	$20 \to 40$	$-$	$-$
h_{γ_n}, dbar	$110 \to 150$	$80 \to 160$	$80 \to 180$	$40 \to 110$	$-$	$80 \to 160$
θ in θ_{min} layer, °C	$\frac{-1.5\to-0.25}{-1.0}$	$\frac{-0.25\to-0.25}{-0.25}$	$\frac{-1.0\to-0.5}{-0.6}$	$\frac{-1.0\to-1.0}{-1.0}$	$\frac{-1.7\to-0.7}{-1.0}$	$\frac{-1.8\to-1.3}{-1.5}$
$p_{\theta_{min}}$, dbar	$80 \to 100$	$80 \to 110$	$70 \to 130$	$50 \to 100$	$50 \to 100$	$50 \to 80$
θ in θ_{max} layer, °C	2.00	2.00	2.00	2.00	2.00	2.00
γ_n at max $(\nabla_n\theta)$	$\frac{27.6\to27.9}{27.7}$	$\frac{27.7\to27.9}{27.75}$	$\frac{27.4\to27.9}{27.75}$	$\frac{27.6\to27.9}{27.75}$	$\frac{27.8\to27.9}{27.8}$	$\frac{27.75\to28.0}{27.8}$
η_{SR3}, m	...	$\frac{0.85\to0.92}{0.88}$	$\frac{0.79\to0.93}{0.89}$	$\frac{0.89\to0.94}{0.94}$	$\frac{0.88\to0.96}{0.91}$	$\frac{0.85\to0.87}{0.86}$
η_{Olbers}, m	...	$\frac{0.84\to0.94}{0.85}$	$\frac{0.80\to0.93}{0.90}$	$\frac{0.91\to0.98}{0.95}$	$\frac{0.88\to1.06}{0.93}$	$\frac{0.88\to0.88}{0.88}$
Southern SACCF						
Position, °S	...	$\frac{64.3\to63.8}{64.1}$	$\frac{64.3\to63.9}{64.1}$	$\frac{63.9\to63.4}{63.6}$	$\frac{63.3\to62.8}{63.1}$	$\frac{64.5\to63.4}{63.9}$
p at $S = 34.5$, dbar	...	$80 \to 120$	$120 \to 110$	$110 \to 110$	$90 \to 120$	$140 \to 110$
p at $S = 34.0$, dbar	...	$0 \to 60$	$50 \to 50$	$40 \to 40$	$70 \to 40$	$-$
h_S, dbar	...	$80 \to 60$	$70 \to 60$	$70 \to 70$	$20 \to 80$	$140 \to 110$
p at $\gamma_n = 27.75$, dbar	...	$60 \to 90$	$60 \to 70$	$65 \to 75$	$10 \to 10$	$100 \to 60$
p at $\gamma_n = 27.25$, dbar	...	$- \to 0$	$0 \to 30$	$30 \to 20$	$-$	$-$
h_{γ_n}, dbar	...	$60 \to 90$	$60 \to 40$	$35 \to 55$	$10 \to 10$	$100 \to 60$
θ in θ_{min} layer, °C	...	$\frac{0\to-0.5}{0}$	$\frac{-1.4\to-0.8}{-1.0}$	$\frac{-1.2\to-0.75}{-1.0}$	$\frac{-1.7\to-1.7}{-1.7}$	$\frac{-1.8\to-1.8}{-1.8}$
$p_{\theta_{min}}$, dbar	...	$70 \to 70$	$50 \to 70$	$50 \to 50$	$70 \to 100$	$50 \to 50$
θ in θ_{max} layer, °C	...	1.80	1.80	1.80	1.80	1.80
γ_n at max $(\nabla_n\theta)$	...	$\frac{27.7\to28.1}{27.9}$	$\frac{27.8\to28.1}{27.9}$	$\frac{27.7\to28.1}{27.85}$	$\frac{27.9\to28.1}{27.95}$	$\frac{27.8\to28.05}{27.9}$
η_{SR3}, m	...	$\frac{0.73\to0.78}{0.75}$	$\frac{0.78\to0.86}{0.82}$	$\frac{0.84\to0.89}{0.86}$	$\frac{0.80\to0.88}{0.84}$	$\frac{0.70\to0.81}{0.77}$
η_{Olbers}, m	...	$\frac{0.72\to0.76}{0.74}$	$\frac{0.77\to0.91}{0.83}$	$\frac{0.78\to0.85}{0.81}$	$\frac{0.82\to0.92}{0.86}$	$\frac{0.75\to0.83}{0.78}$
SB						
Position, °S	$\overline{63.6}$	$\frac{64.8\to64.3}{64.6}$	$\frac{64.8\to64.3}{64.5}$	$\frac{64.3\to63.9}{64.1}$	$\frac{64.8\to63.8}{64.4}$	$\frac{65.4\to64.9}{65.1}$
p at $S = 34.5$, dbar	$230 \to 160$	$150 \to 80$	$170 \to 120$	$170 \to 110$	$170 \to 80$	$230 \to 140$
p at $S = 34.0$, dbar	$20 \to 100$	$10 \to 0$	$50 \to 50$	$30 \to 40$	$-$	$-$
h_S, dbar	$210 \to 60$	$140 \to 80$	$120 \to 70$	$140 \to 70$	$170 \to 80$	$230 \to 140$
p at $\gamma_n = 27.75$, dbar	$80 \to 110$	$70 \to 60$	$60 \to 60$	$50 \to 60$	$- \to 10$	$-$
p at $\gamma_n = 27.25$, dbar	$-$	$-$	$40 \to 0$	$20 \to 30$	$-$	$-$
h_{γ_n}, dbar	$80 \to 110$	$70 \to 60$	$20 \to 60$	$30 \to 30$	$- \to 10$	$-$
θ in θ_{min} layer, °C	$\frac{-1.75\to-1.5}{-1.75}$	$\frac{-1.3\to0}{-1.0}$	$\frac{-1.7\to-1.4}{-1.5}$	$\frac{-1.4\to-1.2}{-1.25}$	$\frac{-1.75\to-1.75}{-1.75}$	$\frac{-1.8\to-1.8}{-1.8}$
θ in θ_{max} layer, °C	1.60	1.30	1.30	1.50	1.60	1.10
γ_n at max $(\nabla_n\theta)$	$\frac{27.6\to28.0}{27.9}$	$\frac{27.7\to28.3}{28.0}$	$\frac{27.8\to28.1}{28.05}$	$\frac{27.7\to28.1}{28.0}$	$\frac{27.85\to28.1}{28.0}$	$\frac{27.9\to28.15}{28.05}$
η_{SR3}, m	...	$\frac{0.69\to0.73}{0.70}$	$\frac{0.70\to0.78}{0.74}$	$\frac{0.78\to0.84}{0.81}$	$\frac{0.75\to0.83}{0.77}$	...
η_{Olbers}, m	...	$\frac{0.67\to0.72}{0.70}$	$\frac{0.70\to0.77}{0.73}$	$\frac{0.75\to0.78}{0.76}$	$\frac{0.77\to0.82}{0.78}$	...
ASF						
Position, °S	$\overline{64.5}$	$\overline{64.6}$	$\frac{65.6\to65.1}{65.4}$	$\frac{65.6\to65.1}{65.4}$	$\frac{65.4\to64.8}{65.1}$	$\frac{65.6\to65.4}{65.5}$
p at $\theta = 0$ °C, dbar	$150 \to 570$	$60 \to 220$	$200 \to 450$	$250 \to 750$	$200 \to 400$	$180 \to 560$
θ_{min}, °C	-1.75	-1.3	-1.5	-1.5	-1.75	-1.8

See Table 4 for explanation of symbols.

Table 6
Summary of front indicators for the Australian sector of the Southern Ocean

Front	Indicator
STF	$\theta = 11$ °C at $p = 150$ dbar
SAF-N	max $(\nabla_h \theta)$ at $p = 400$ dbar in θ range [6·8] °C
SAF-M	max $(\nabla_h \theta)$ at $p = 400$ dbar in θ range [5·6] °C
SAF-S	max $(\nabla_h \theta)$ at $p = 400$ dbar in θ range [3·5] °C
PF-N	$\theta = 2.0$ °C in θ_{min} layer
PF-S	$\theta = 2.2$ °C in θ_{max} layer
SACCF-N	$\theta = 2.0$ °C in θ_{max} layer
SACCF-S	$\theta = 1.8$ °C in θ_{max} layer
SB	max $(\nabla_h \theta)$ in θ_{max} layer for the θ range [1·1.75] °C
ASF	$\theta = 0$ °C at $p = 200$ dbar

(Table 5, Fig. 4). The maxima in along-isopycnal gradients occur at greater density as each of the fronts is crossed from north to south.

4. Front positions and variability in the Tasmanian sector

The relatively large number of high resolution repeat hydrographic sections south of Tasmania has allowed us to look in detail at the structure and variability of the fronts. However, the sections are limited to a single line and provide no information about frontal structure to the east and west of the cruise track. Moreover, while the data set includes at least one section in each season, six sections over 5 years are inadequate to sample the variability of the fronts. In this section, we show that the fronts can be identified in maps of sea surface height (SSH), and then use these maps to determine the path and variability of each of the fronts in the Tasmanian sector (130–160°E).

4.1. Correspondence between SSH and the density field

Each of the deep-reaching ACC fronts at SR3 corresponds to a narrow range of sea surface height (SSH) values (Tables 3–5). Two examples, from January 1995 and September 1996, demonstrate the

extent to which the detailed structure of the density field is reflected in SSH (Fig. 12). Figs. 2c and 11 show the corresponding neutral density sections.

The SSH maps reflect each feature in the density field which extends over a substantial portion of the water column. For example, the deep isopycnal bowl in the Subantarctic Zone in January 1995 (Fig. 2c) coincides with a high in SSH with a maximum of 2.15 m between 46° and 49°S (Fig. 12a). The two bands of high density gradient at 50° and 51.5–52°S corresponding to the northern and southern branches of the SAF coincide with large SSH gradients at these latitudes. These two fronts are separated by a narrow band of isopycnals sloping in the opposite direction (Fig. 2c), which is reflected in the "reverse S" shaped bend of the 1.70-m contour in Fig. 12a.

The shallow isopycnal bowl centered at 57°S in Fig. 2c corresponds to an S-shaped bend in the 1.25-m SSH contour. Further south, the southern branch of the PF corresponds to a broad front where isopycnals shoal to the south between 58.5° and 60°S. The SPF is evident in SSH as an enhanced gradient between the 1.05- and 1.15-m contours between these latitudes. The branches of the SACCF evident in the density field at 62.5° and 63.5°S, and the reversal of slope between the two branches, coincide with weak SSH gradients and a meander of the 0.95-m contour.

A second example, illustrating the SSH field corresponding to the somewhat different frontal structures observed in September 1996 is shown in Fig. 12b. An intense cyclonic eddy is seen at 49°S in the SSH map, just to the west of SR3. The section just clips the eastern side of the eddy, resulting in a weak doming of the isopycnals at this latitude (Fig. 11). Three branches of the SAF are evident in both the density field and SSH: the northern branch at 50.5°S coincides with the 1.95-m contour, the middle branch at 51.5°S with the 1.75-m contour, and the southern branch at 53°S with the 1.50-m contour.

Applying the customary definition of the PF (the northernmost extent of θ_{min} water cooler than 2 °C near 200-m depth) to identify the front on the September 1996 occupation of SR3 is complicated by the presence of two eddies pinched off from the front. A small pool of T-min water < 2 °C just north
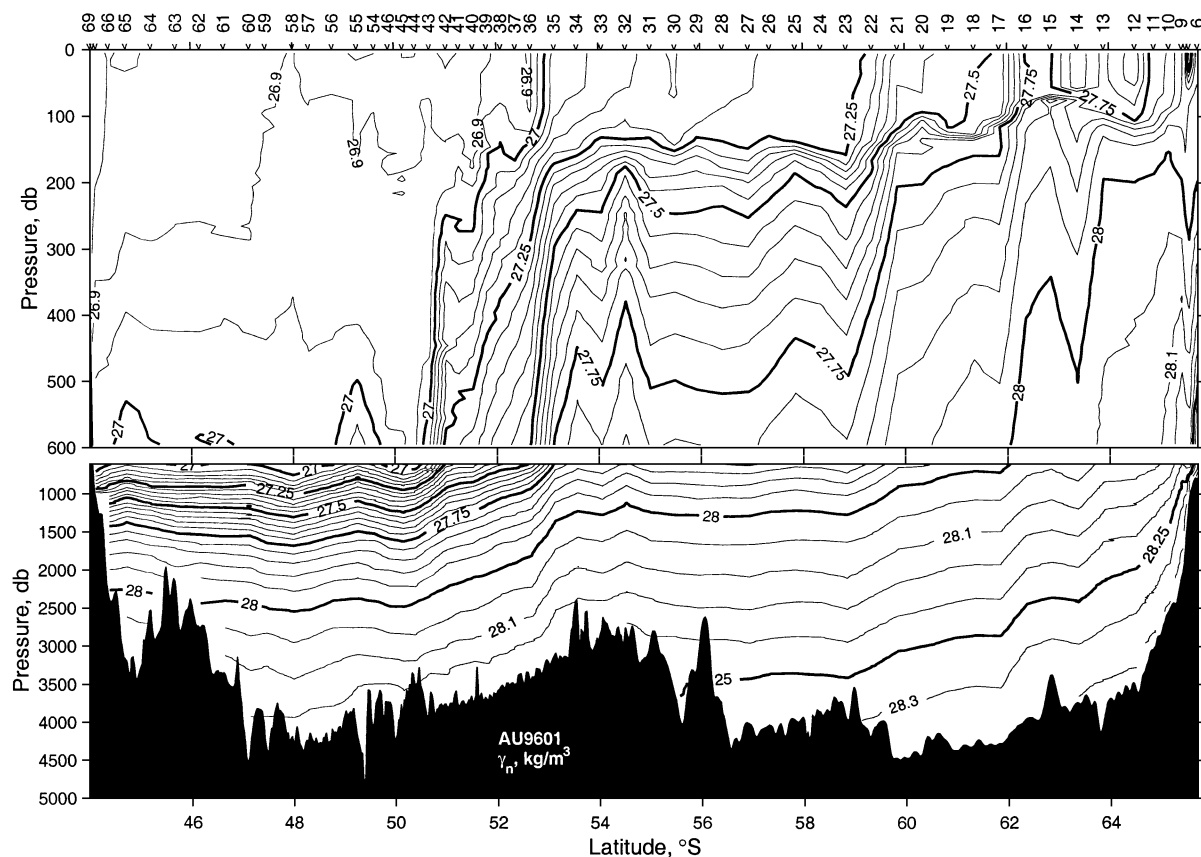
Fig. 11. Neutral density anomaly (γ_n, in kg m^{-3}) on the September 1996 occupation of SR3.

of 54°S coincides with a meander of the 1.35-m contour. A larger isolated pool of $\theta_{min} < 2$ °C water just south of 54°S corresponds to a cyclonic eddy centered just to the west of the section. The strongest signature of the northern PF in the SSH map is seen at 55°S, where the 1.25- to 1.45-m contours are clustered and oriented roughly parallel to SR3, consistent with the weak density signature of the front in the corresponding density section. The flat isopycnals between 55° and 59°S are reflected in an equally flat region of the SSH map. The horizontal density gradient across the southern PF at 59°S (Fig. 11) is more intense than on the January 1995 section (Fig. 2c). This is also reflected in the SSH maps, where the gradient of SSH across the southern PF is about three or four times larger in September 1996 than in the earlier section. The two branches of the SACCF at 62° and 64°S, and the reversal of slope

between the two, again are evident in both the density field and SSH map.

The comparison of Figs. 2c and 11 to Fig. 12 shows that each of the significant features of the density field at SR3 is also evident in SSH, and that each front corresponds to a particular axial value of SSH (Tables 3–5). In Fig. 12, these axial values are highlighted to illustrate that these SSH contours usually correspond to fronts throughout the Tasmanian sector. This can be seen more clearly in Fig. 13, in which the same SSH contours are overlaid on a map of SSH gradients from the period of the January 1995 section. The SSH contours generally correspond to regions of enhanced $\nabla\eta$ not just at SR3 but along their entire path. While there are some exceptions (both regions of high gradient that do not correspond to one of the selected SSH contours, and locations where the SSH contours

coincide with relatively low gradients), maps of SSH apparently provide a reasonable guide to the location of the major fronts in this sector.

Fig. 13 shows three distinct fronts between 48° and 54°S west of 140°E. The northern and middle filaments merge near 140°E to form the northern branch observed at SR3. The southern branch, which is found about 1.5° south of the northern branch at SR3 (Table 3), lies more than 5° of latitude to the south of the northern branch at 130°E. Just downstream of the SR3 line, all three branches of the SAF have merged again. Between SR3 and the Macquarie Ridge at 160°E, the SAF meanders vigorously over a 5° latitude band and a number of pinched off rings can be seen. The SSH map in September 1996 (Fig. 12b) shows a similar pattern. At 130°E, three distinct filaments of the SAF can be seen, with a separation of about 5° of latitude. The filaments tend to merge further east, although at this time, three distinct bands of enhanced gradient can still be identified, as described above. The September 1996 map also shows a wide band of intense meandering and eddy-shedding between SR3 and the Macquarie Ridge at 160°E.

4.2. Location and variability of fronts in the 130°E to 160°E sector

Having demonstrated that fronts can be identified in maps of SSH, we can use the altimeter data to map the fronts in the Tasmanian sector every 10 days between 1992 and 2002. Fig. 14 shows the SSH contours corresponding to three branches of the SAF, two branches of the PF, two branches of the SACCF, and the SB. A contour is plotted for each front every 120 days between 1992 and 2000, so that each realization of the front location is independent. (The value of 120 days is subjective, but likely conservative given the 20–30-day integral time scale estimated from 2-year current meter records in the SAF at SR3 (Phillips and Rintoul, 2000).) To simplify the plot, closed rings are eliminated by plotting only contours, which extend across the full width of the sector. Fig. 14a shows the "meander envelope" of each of the fronts, but not the distribution within the envelope; Fig. 14b displays the same information as a two-dimensional

histogram of the frequency of occurrence of a given height contour at each latitude along that meridian. Shaded regions in Fig. 14b indicate that the front is present at that location more than 20% of the time. Fig. 14 gives a qualitative indication of the location and variability of the fronts, as a particular SSH value does not always coincide with an enhanced gradient at all locations and times (e.g. Fig. 13).

At the SR3 section, the front locations inferred from the 7-year altimeter record agree with those estimated from the six hydrographic sections: the northern SAF is found between 50° and 51°S, the southern SAF between 52° and 53°S, the northern PF between 53° and 54°S, the southern PF between 58.5° and 60°S, the SACCF at 62°S and 64°S, and the SB between 64° and 65°S.

The northern SAF, which is north of the Southeast Indian Ridge (SEIR) throughout the sector, slopes slightly south of east between 130° and 160°E. Each of the other contours plotted enters the sector across 130°E to the south of the ridge crest. As each front encounters the shoaling topography of the ridge, it is deflected equatorward, consistent with fluid columns attempting to conserve their planetary vorticity. The equatorward deflection begins progressively further east for the southern fronts, reflecting the northwest to southeast trend of the ridge. After crossing the ridge, each of the fronts shifts back to the south.

Fig. 14 confirms the multi-filamented structure of the SAF. While at SR3, the envelope of SSH contours corresponding to the middle and southern SAF tends to overlap, consistent with the fact that only one occupation of SR3 (September 1996) showed a separate middle SAF, three distinct filaments can be seen between 130° and 137°E. Three bands of high $\nabla \eta$ can be also seen at these longitudes in the synoptic maps in Figs. 12 and 13. The filaments are not completely fixed in terms of the range of SSH spanned by each current core: individual height contours sometimes split from one filament and join another further downstream. In the eddy-rich region east of SR3 (Fig. 1), the meander envelopes of all three branches of the SAF are broad and overlapping. Fig. 14 also confirms that the northern PF runs roughly parallel to SR3 between 53° and 56°S.

The width of the "meander envelope" of each front varies with longitude. For example, the position

of the southern SAF varies by less than 1° of latitude on the SR3 line, consistent with the in situ data, but meanders over 3° of latitude to the east and west. Likewise, the meridional displacements of the northern and southern PF are a minimum at the SR3 line (< 1° of latitude) and larger to the east and west. The location of the northern branch of the SACCF, in contrast, is more variable at SR3 than to the east and west. The stability of the location of a front on a single section like SR3 is not necessarily a good indicator of the extent to which the front may meander at some other longitude.

In particular, the tendency for fronts to meander appears to be strongly influenced by the bathymetry.
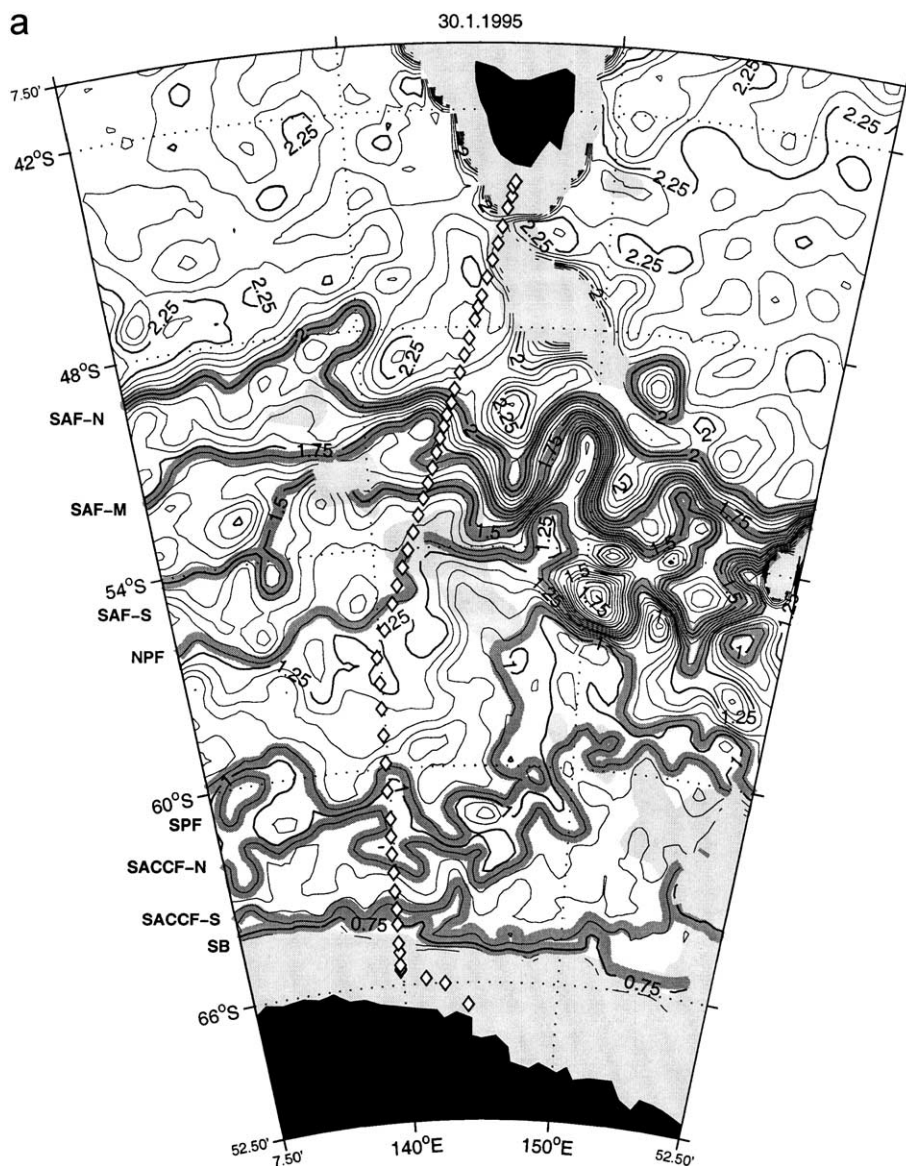
Fig. 12. Sea surface height (m) at the time of the (a) January 1995 and (b) September 1996 occupations of SR3. The thick grey contours indicate height contours which coincide with the fronts identified at SR3 (see labels on left side of plot).
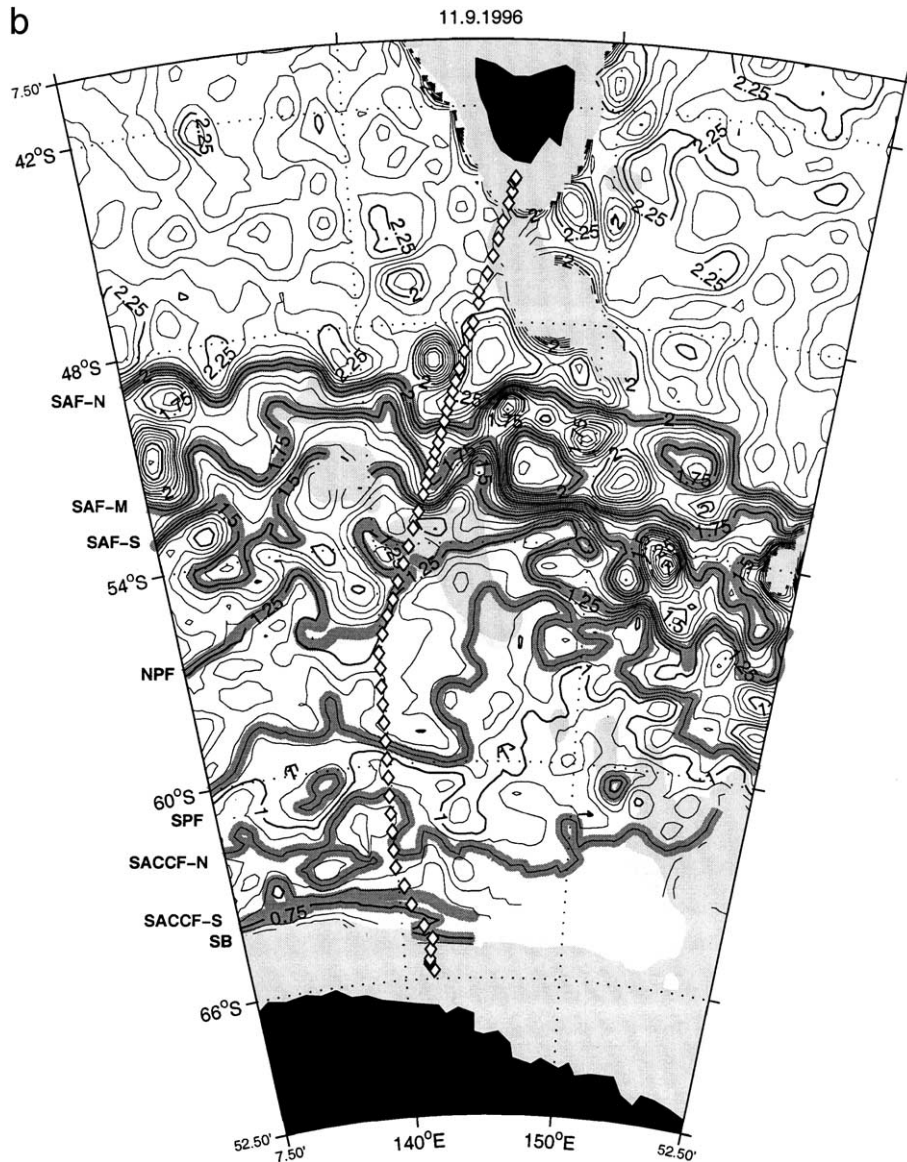
Fig. 12 (*continued*).

Where each of the fronts crosses the ridge crest, the meander envelope is narrow; where the fronts cross deep basins or flow parallel to a zonal ridge, the distribution is moderately narrow; downstream of significant topographic obstructions, the meander envelope is broad. In addition to this response to the large-scale bathymetry, the flow also responds to smaller-scale features. For example, each of the fronts crosses the ridge at a particular fracture zone or low point in the ridge (Fig. 14c). In this figure, the modal paths of the fronts (derived from Fig. 14b) are shown with the underlying topography. For some of the fronts, the frequency distributions are clearly bimodal. For example, near 139° E, the southern branch of the SAF sometimes crosses the SEIR south of a high point on the ridge at 52–52.5°S, and more
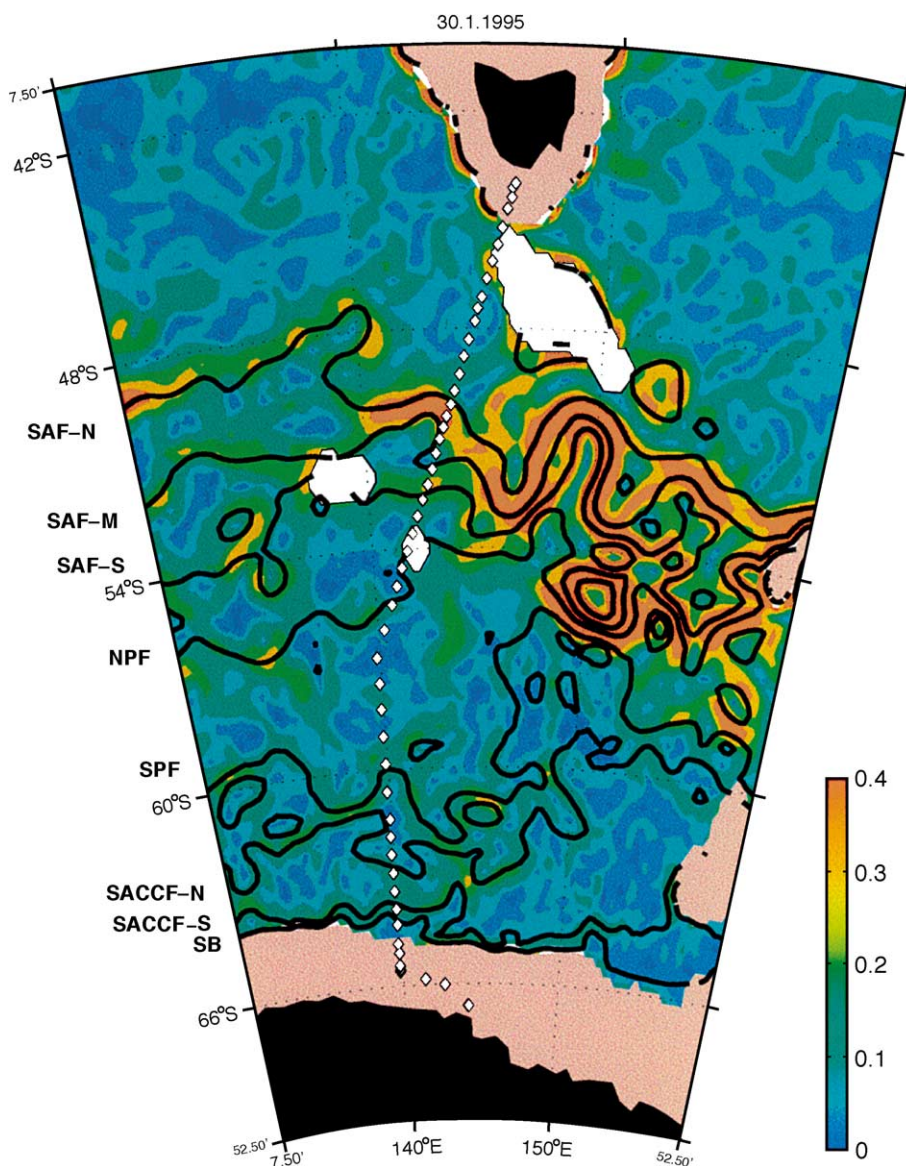
Fig. 13. Gradient of sea surface height at the time of the January 1995 occupation of SR3 (color), with selected height contours corresponding to particular fronts on SR3 overlaid (bold lines).

frequently to north of the high point, where the southern and middle branches of SAF merge.

5. Interannual variability of front locations

The six repeats of SR3 are not sufficient to define the interannual variability in the location of the fronts.

The altimeter maps provide a useful guide to the spatial and temporal variability in the front locations, but are qualitative in the sense that any given height contour does not always coincide with a large horizontal gradient. However, analysis of the SR3 sections shows that the fronts can be identified reliably using subsurface temperature (i.e. the temperature-based criteria summarized in Table 6 coincide with front

positions defined from maxima in transport and lateral gradients, Figs. 5–10). Therefore, we can use the 45 XBT sections collected between 1992 and 1999 to look for evidence of temporal variability in front locations. The six XBT sections obtained each field

season generally span the summer half of each year (October to March). Sokolov and Rintoul (submitted for publication 2001) demonstrated that averages of XBT sea surface temperature over each austral summer season shows a similar interannual signal to

a
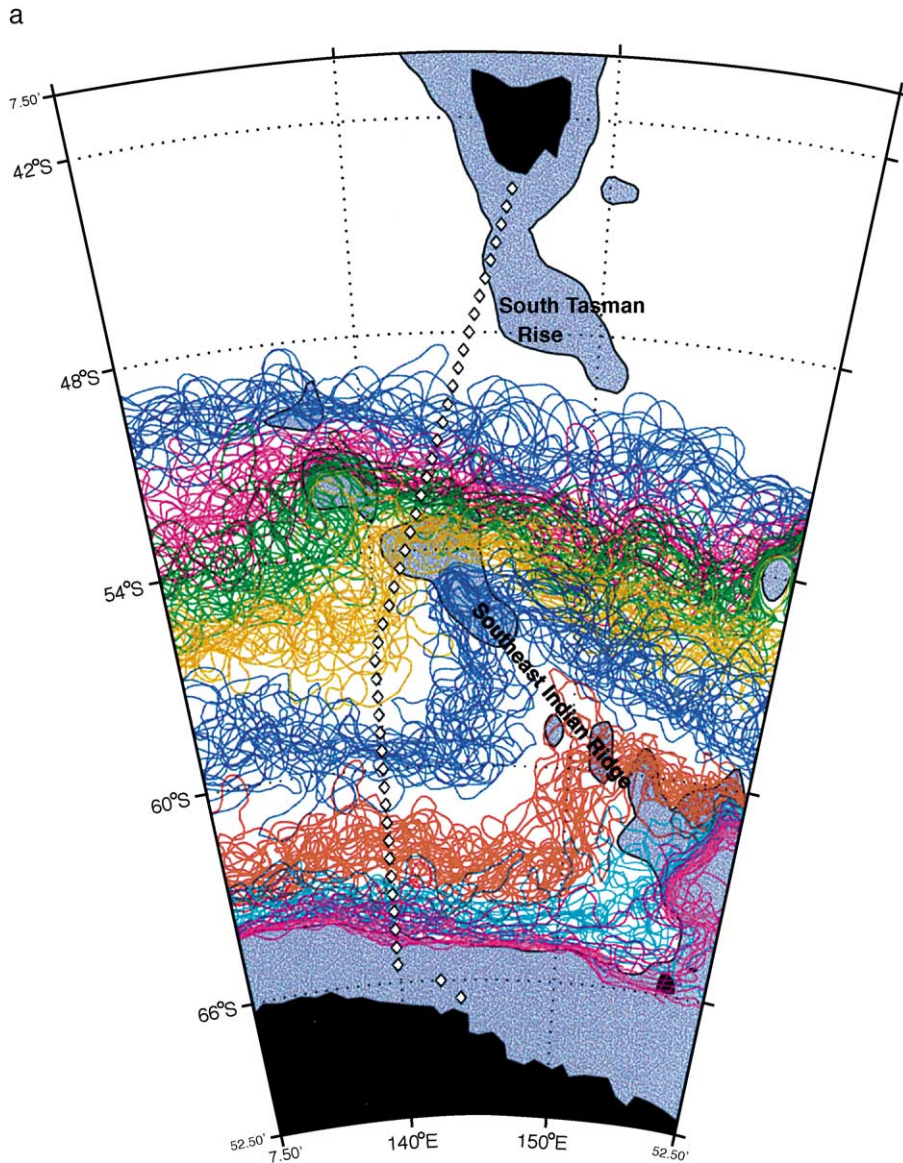
Fig. 14. (a) SSH contours corresponding to each front in the Tasmanian sector, plotted every 120 days for the period between 1992 and 2000. Contours plotted: 1.9 m (SAF-N, blue), 1.7 m (SAF-M, magenta), 1.45 m (SAF-S, green), 1.3 m (PF-N, yellow), 1.1 m (PF-S, blue), 0.9 m (SF-N, red), 0.8 m (SF-S, cyan), 0.75 m (SB, magenta). (b) The frequency of occurrence of a particular height contour at each grid point. The thin lines indicate the envelope which includes the height contour 6% of the time; the shaded regions include the front more than 20% of the time. Colors as in (a). (c) Modal paths of contours shown in panels (a) and (b).
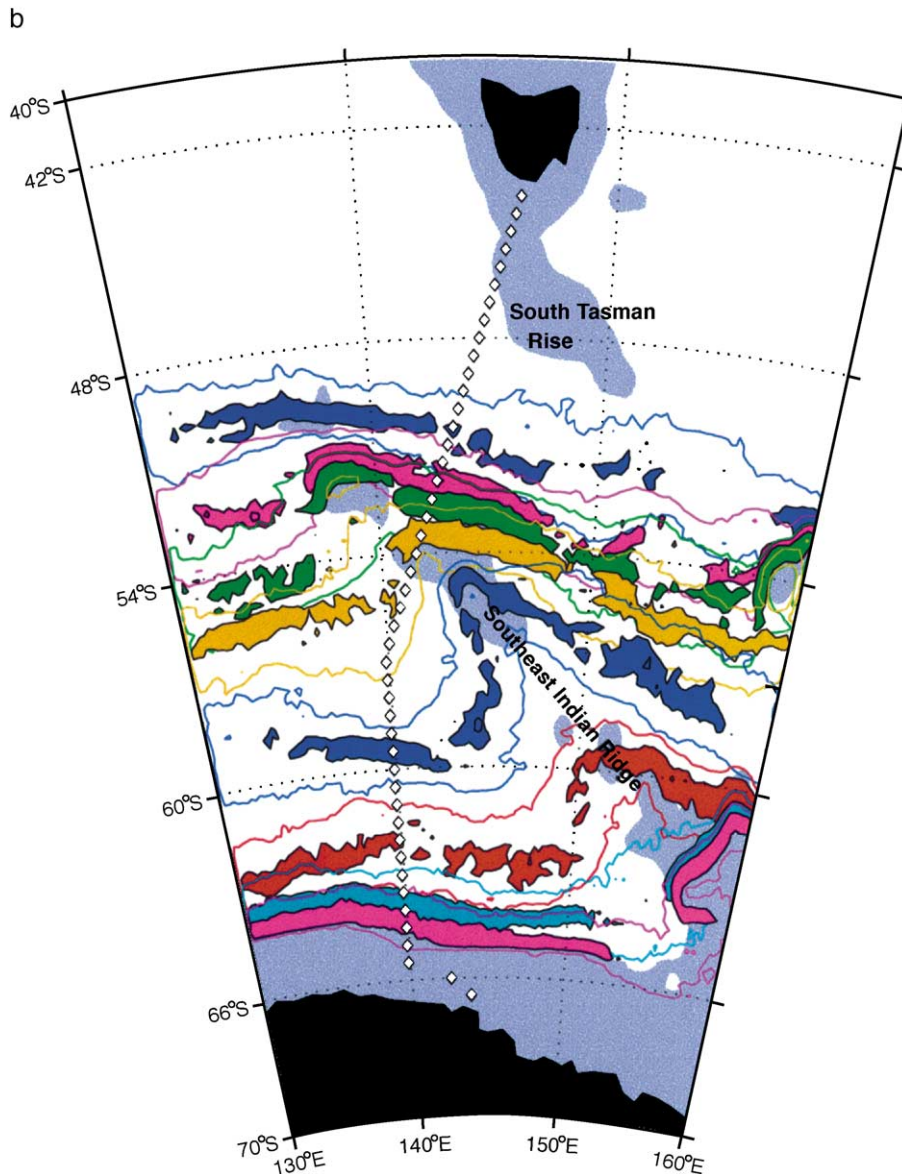
Fig. 14 (*continued*).

continuous satellite measurements of SST which have been low-pass filtered. Interannual changes in the location of the fronts can therefore be assessed from the XBT data using the criteria in Table 6.

The latitude of most of the fronts varies from year to year (Fig. 15). The latitude of the STF oscillates by about ± 1° about its mean position, with an apparent period of about 4 or 5 years (the time scale of the oscillation is of course not resolved in such a short record). (Note that the variability in position of the STF is larger than that inferred from the six SR3 repeats; this reflects both larger variability along the XBT cruise track and the fact that the six sections did not capture all the variability in the front.) The northern branch of the SAF is furthest north in 1996–1997, and furthest south in 1993–1994 and
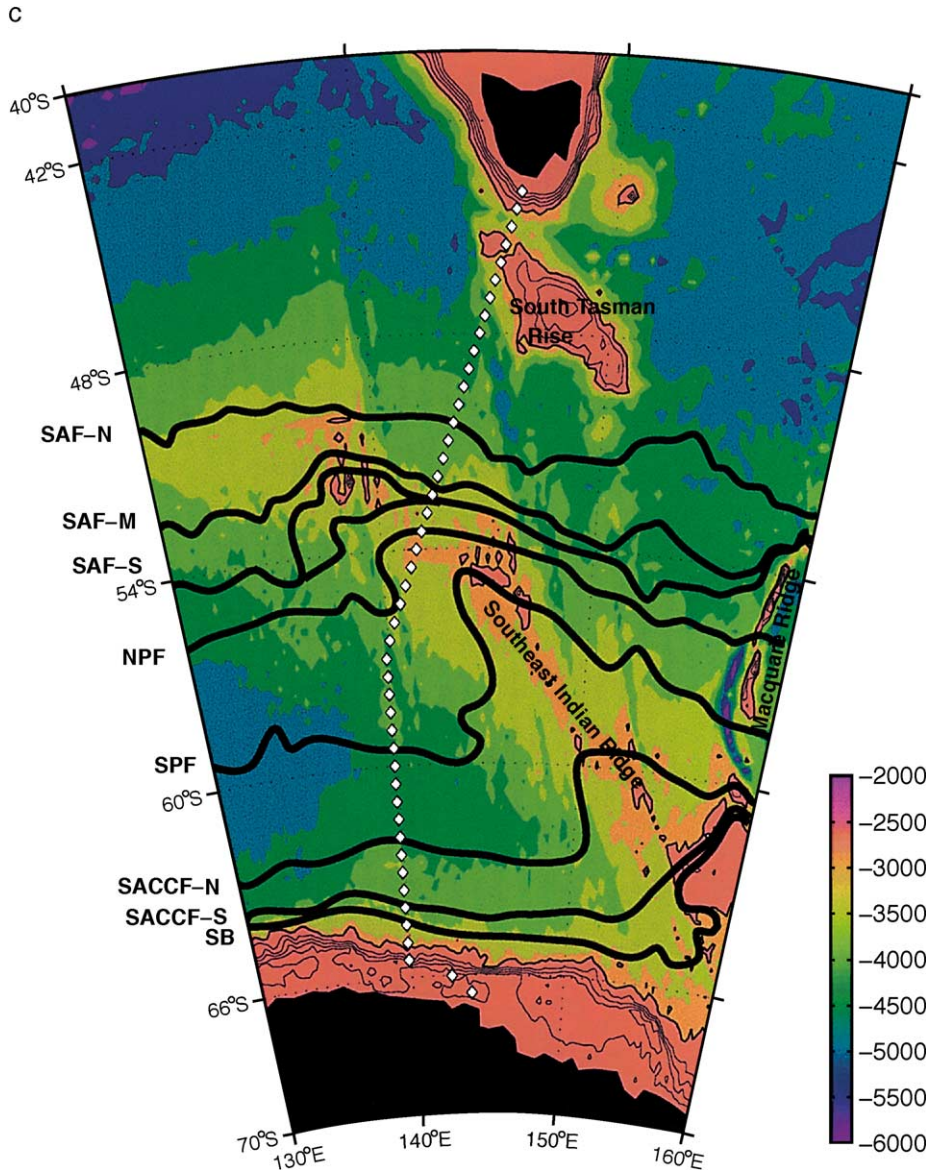
Fig. 14 (*continued*).

1998–1999, with meridional displacements about half those of the STF. The mean position of the southern branch of the SAF does not change much from year-to-year, but changes substantially within individual years (e.g. by 3° of latitude in 1996–1997). The NPF, in contrast, shows little variation within each austral summer, but varies moderately between years (by ± 0.5°). The mean position of the

SPF varies from year to year by a similar amount, and like the STF reaches its northernmost position in 1994–1995 and 1995–1996. The two branches of the SF also reach their northernmost mean position in 1995–1996.

Also plotted in Fig. 15 is the SST at the mean latitude of each front in each austral summer season. At each of the fronts, the movements of the fronts
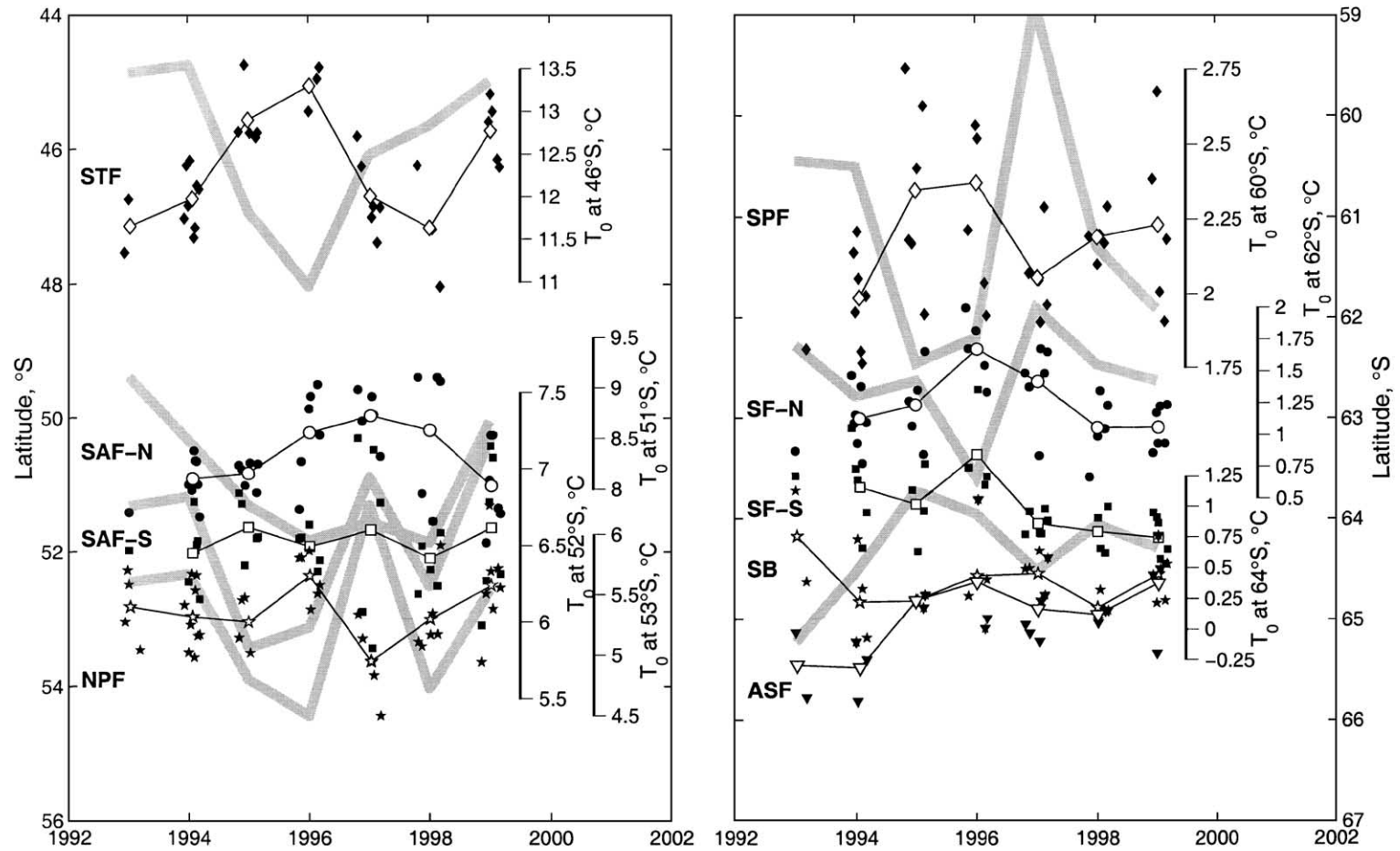
Fig. 15. Interannual variability in the latitude of fronts at XBT line (symbols). Season-averaged front locations are shown by back lines with open symbols. Thick grey lines indicate the sea surface temperature at the mean latitude of each front, averaged over each austral summer field season (October to March).

and the SST are anti-correlated: northward front displacements are associated with cooler than average temperatures, as expected given that temperature decreases to the south across each front. The significant point is that meridional shifts of the fronts can explain much of the SST variability in the Southern Ocean, as discussed in more detail by Sokolov and Rintoul (submitted for publication). They show that displacements of the fronts may be an important aspect of the coupled physics of the Antarctic Circumpolar Wave.

6. Discussion

Fronts are ubiquitous, robust, circumpolar features of the Southern Ocean. On every transect with sufficient horizontal resolution, the property fields are found to be organized such that the transition from warm salty water in the north to cool fresh water in the south occurs in a series of steps, or bands of enhanced lateral gradient. These fronts accomplish most of the transport of the ACC, and delineate zones characterized by distinct biogeochemical distributions.

The increase in availability of high quality hydrographic sections, remote sensing, and high resolution models have made it clear that the frontal structure of the Southern Ocean is complex: fronts can split into multiple filaments, or merge to form "super-fronts". As a result, circumpolar maps of mean SST gradients (e.g. Hughes et al., 1998) make the ACC look more akin to a braided river in a broad valley than it does to the simple three-front picture developed from Drake Passage experience. Dynamical instabilities of Southern Ocean fronts introduce spatial and temporal variability, which further complicates attempts to use simple phenomenological indicators to locate individual fronts.

Nevertheless, we find that the fronts south of Tasmania can be consistently defined using a variety of criteria. The ACC fronts are associated with enhanced lateral density gradients, which extend throughout the water column and are therefore associated with transport maxima. Front locations defined using maxima in transport and lateral gradients (both on isobars and isopycnals) are generally consistent with positions inferred from other criteria used by earlier investigators. For example, the descent of the

AAIW salinity minimum is commonly used to locate the SAF. We find the descent of the salinity minimum indeed coincides with the SAF, but because the salinity minimum deepens over several degrees of latitude, this indicator used in isolation leaves some ambiguity in the position of the front. At SR3, two transport maxima are consistently found in the latitude band where the salinity minimum deepens to the north.

Relying on transport and lateral gradient maxima to identify fronts, we find that each of the major ACC fronts consists of multiple branches at SR3. Each branch can be found on each section using a consistent set of indicators. The latitude of each branch or filament is relatively stable in time, typically varying by $\pm 0.5°$ of latitude at SR3. Rintoul and Sokolov (2001) found that the baroclinic transport of each of the fronts was also very steady based on the six repeat sections. The relative steadiness of the front locations at SR3 is not, however, typical of the Tasmanian sector as a whole: maps of frontal variability obtained from satellite altimetry suggest that both up- and downstream of SR3 the fronts meander over a broader latitude range.

The results presented here provide a somewhat different view of the structure of the SAF to that presented by Phillips and Rintoul (in press) on the basis of 2-year current meter records on the SR3 line. By averaging the current meter measurements in a stream-coordinate defined using temperature, they estimated a mean cross-stream profile of absolute velocity in the SAF. The resulting profile shows a single maximum, not the two jet structure apparent in the repeat sections. To do the stream wise averaging, an assumption is made that the cross stream structure of the current does not change with time. Phillips and Rintoul found that this assumption did not hold as well in the ACC as Hall and Bryden (1985) found for the Gulf Stream. The repeat sections reveal why this is so: the cross stream structure is not entirely fixed, but rather varies somewhat as the frontal filaments merge and split. In the 2-year mean, the distinct transport maxima usually evident in the synoptic sections in Figs. 5–10 are smoothed to form one broader peak.

Overall, the analysis of repeat hydrographic and XBT sections and satellite altimetry underscores the complex, multi-filamented structure of the ACC south of Australia. Given this complexity, it is remarkable that simple scalar criteria such as those identified by

various investigators over the last century work as well as they do. For example, a deep-reaching current core coincides with the northernmost extent of temperature minimum water cooler than 2 °C, the usual indication of the PF, throughout almost the entire Southern Ocean (Botnikov, 1963; Belkin and Gordon, 1996). This is despite the fact that the PF splits into multiple branches at some locations, and at others merges with other fronts, to later diverge again with its "identity" intact. The robust, large-scale frontal structure of the ACC reflects the response to large-scale forcing by winds and buoyancy exchange, the presence of a deep circumpolar channel, baroclinic and barotropic instability, and perhaps other factors, but a complete dynamical explanation of the ACC fronts remains elusive.

Recent high resolution sections and remote sensing have confirmed that the fronts are strongly influenced by bathymetry. For example, Moore et al. (1999) have used satellite SST data to show how the path and structure of the PF is influenced by sea-floor topography. The fronts of the Southern Ocean extend throughout the water column and so interact with the bathymetry. Over broad deep abyssal plains, the fronts tend to be relatively weak and free to meander over a wide latitude range (e.g. in the southeast Pacific). Near steep topography, the fronts are sharper and less prone to meander. As suggested by Fig. 14, the mean path of the fronts is determined to a large extent by the attempt of fluid columns to navigate the complicated geometry of the ocean basins while conserving their potential vorticity. The interaction of the fronts of the ACC with the bottom topography is central to the dynamics of the current as a whole: the momentum supplied by the wind is balanced by topographic torques where deep currents interact with the sea floor (see Rintoul et al. in press(a) for a discussion).

We have found satellite altimeter maps of SSH to be of great value for synoptic mapping of Southern Ocean fronts. Even relatively weak and small-scale features of the density field are reflected in SSH. This correspondence supports the conclusion of Rintoul et al. (in press(b)) that the altimeter signal primarily reflects changes in the full-depth baroclinic field. After confirming that particular SSH values tend to coincide with individual fronts, the SSH maps were particularly useful for mapping fronts and their variability across the Tasmanian sector. The maps con-

firm the multi-branched nature of the fronts in this region.

Our aim in this study has not been to identify as many frontal filaments as possible. We believe the addition of new fronts and indicators has the potential to increase confusion in a field in which the multiplicity of definitions already causes some difficulties, and so should be avoided where possible. However, precision is required if results of different studies are to be compared in a consistent manner. The detailed summary of criteria corresponding to each front provided in Tables 2–6 we hope will provide useful guidance to future investigators making such comparisons in this and other sectors. More importantly, the multiple branches identified in this study and others are robust, distinct features of the circulation. Improvement in our understanding of the dynamics and origin of the fronts of the Southern Ocean requires accurate descriptions of the location, structure and variability of the fronts, as we have attempted to do for the region south of Tasmania.

7. Summary

We have used a comprehensive data set spanning almost a decade to describe the structure of the Southern Ocean fronts south of Tasmania. The availability of six repeat, high quality hydrographic sections with spatial resolution as fine as 30 km across the major fronts has allowed us to examine the fronts in detail. When defining the fronts, we have placed most weight on the distribution of horizontal gradients of various properties, and the distribution of transport. In general, fronts defined in this way correspond to various scalar criteria used by earlier investigators. The existence of suitable proxies expressed in terms of subsurface temperature or SSH has allowed us to examine the spatial and temporal variability of the front locations using the longer and more continuous time series of XBT sections and satellite altimetry. The results can be summarized as follows:

– The STF lies between 44.5° and 45.6°S on SR3. The shallow, nearly density-compensating nature of the thermohaline gradients results in weak flow and the STF is therefore not associated with an eastward transport maximum.

- The SAF consists of multiple branches in the Tasmanian sector. Three branches can be identified west of SR3 in SSH maps. Two of the branches have generally merged by the longitude of SR3, leaving two cores with mean latitudes of $50.5°$ and $52-53°$S. Both branches are characterized by relatively narrow meander envelopes at SR3, and much more vigorous meandering between SR3 and the Macquarie Ridge at $160°$E.
- The PF also consists of two branches on every occupation of SR3. The northern branch crosses the section at a mean latitude of $53.5°$S. The northern PF executes an S-shaped turn just to the west of SR3, so that the flow is more or less parallel to the section between $54°$ and $56°$S. The southern branch is found between $58°$ and $60°$S on every SR3 section.
- Four fronts are consistently found south of the southern PF. The SACCF consists of branches at $62°$ and $64°$S, which are frequently connected by streamlines, which turn back to the west between them. The SB is typically a distinct feature found between $64°$ and $65°$S, but is sometimes adjacent to the SACCF. The ASF is found over the upper continental slope of Antarctica.
- Maps of SSH illustrate the extent to which each of the fronts is influenced by the bottom topography. The fronts tend to shift equatorward as the bottom shoals, to become tighter in the vicinity of steep topography, and to meander vigorously in the deep basins downstream of topographic obstacles.
- The latitude of the fronts varies from year-to-year, as assessed from 7 years of austral summer (October to March) repeat XBT sections. Meridional displacements of the fronts are correlated with variations in SST, suggesting shifts of the fronts contribute to SST variability observed on interannual time scales.

Acknowledgements

References

Belkin, I.M., Gordon, A.L., 1996. Southern ocean fronts from the Greenwich Meridian to Tasmania. J. Geophys. Res. 101, 3675–3696.

Botnikov, V.N., 1963. Geographical position of the Antarctic convergence zone in the Pacific Ocean. Sov. Antarct. Exped. Inf. Bull., Engl. Trans. 4, 324–327.

Buinitsky, V., 1973. Sea Ice and Icebergs of the Antarctic (in Russian). Izd. LGU, Leningrad, 256 pp.

Burling, R.W., 1961. Hydrology of circumpolar waters south of New Zealand. N. Z. Dep. Sci. Ind. Res. Bull. 149, 66 pp.

Callahan, J.E., 1972. The structure and circulation of Deep Water in the Antarctic. Deep-Sea Res. 19, 563–575.

Clifford, M.A., 1983. A descriptive study of the zonation of the Antarctic Circumpolar Current and its relation to wind stress and ice cover. Master's thesis, Texas A&M University, College Station, 93 pp.

Deacon, G.E.R., 1937. The hydrology of the southern ocean. Discov. Rep. 15, 1–124.

de Baar, H.J.W., 1995. Importance of iron for plankton blooms and carbon dioxide drawdown in the Southern Ocean. Nature 373, 412–415.

Garner, D.M., 1967. Hydrology of the south-east Tasman Sea. N. Z. Oceanog. Inst. Mem. 48, 40 pp.

Gordon, A.L., 1967. Structure of Antarctic waters between $20°$W and $170°$W. Am. Geogr. Soc. Antarct. Map Folio Ser., Folio 6, 10 pp.

Gordon, A.L., 1971. The Antarctic Polar Front zone. In: Reid, J.L. (Ed.), Antarctic Oceanology I. Antarctic Research Series, vol. 15. American Geophysical Union, Washington, DC, pp. 205–221.

Gordon, A.L., Taylor, H.W., Georgi, D.T., 1977. Antarctic oceanographic zonation. In: Dunbar, M.J. (Ed.), Polar Oceans. Arctic Institute of North America, Calgary, pp. 45–76.

Hall, M.M., Bryden, H.L., 1985. Profiling the gulf stream with a current meter mooring. Geophys. Res. Lett. 12, 203–206.

Hughes, C., Jones, M., Carnochan, S., 1998. Use of transient features to identify eastward currents in the Southern Ocean. J. Geophys. Res. 103, 2929–2944.

Jackett, D.R., McDougall, T.J., 1997. A neutral density variable for the World's Oceans. J. Phys. Oceanogr. 27, 237–263.

Le Traon, P., Nadal, F., Ducet, N., 1998. An improved mapping method of multisatellite altimeter data. J. Atmos. Ocean. Technol. 15, 522–534.

Moore, J., Abbott, M., Richman, J., 1999. Location and dynamics of the Antarctic Polar Front from satellite sea surface temperature data. J. Geophys. Res. 104, 3059–3073.

Nagata, Y., Michida, Y., Umimura, Y., 1988. Variations of positions and structures of the ocean fronts in the Indian Ocean Sector of the Southern Ocean. In: Sahrhage, D. (Ed.), Antarctic Ocean and Resources Variability. Springer-Verlag, Berlin, pp. 92–98.

Nowlin Jr., W.D., Clifford, M., 1982. The kinematic and thermohaline zonation of the Antarctic Circumpolar Current at Drake Passage. J. Mar. Res. 40, 481–507 (Supplement).

Nowlin Jr., W.D., Klinck, J.M., 1986. The physics of the Antarctic Circumpolar Current. Rev. Geophys. Space Phys. 24, 469–491.

Nowlin Jr., W.D., Whitworth III, T., Pillsbury, D., 1977. Structure and transport of the Antarctic Circumpolar Current at Drake Passage from short-term measurements. J. Phys. Oceanogr. 7, 788–802.

Olbers, D., Gouretski, V., Seiß, G., Schröter, J., 1992. Hydrographic Atlas of the Southern Ocean Alfred Wegener Institute for Polar and Marine Research, Bremerhaven. 17 pp. + 82 plates.

Orsi, A.H., Whitworth III, T.W., Nowlin Jr., W.D., 1995. On the meridional extent and fronts of the Antarctic Circumpolar Current. Deep-Sea Res., Part I 42, 641–673.

Peterson, R.G., Stramma, L., 1991. Upper-level circulation in the South Atlantic Ocean. Prog. Oceanogr. 26, 1–73.

Phillips, H.E., Rintoul, S.R., 2000. Eddy variability and energetics from direct current measurements in the Antarctic Circumpolar Current south of Australia. J. Phys. Oceanogr. 30, 3050–3076.

Phillips, H.E., Rintoul, S.R., 2001. A mean synoptic view of the Subantarctic Front south of Australia. J. Phys. Oceanogr. 32, 1536–1553.

Read, J.F., Pollard, R.T., Morrison, A.I., Symon, C., 1995. On the southerly extent of the Antarctic Circumpolar Current in the southeast Pacific. Deep-Sea Res., Part II 42 (4–5), 933–954.

Rintoul, S.R., Bullister, J.L., 1999. A late winter hydrographic section from Tasmania to Antarctica. Deep-Sea Res., Part I 46, 1417–1454.

Rintoul, S.R., Sokolov, S., 2001. Baroclinic transport variability of the Antarctic Circumpolar Current south of Australia (WOCE repeat section SR3). J. Geophys. Res. 106, 2795–2814.

Rintoul, S.R., Trull, T.W., 2001. Seasonal evolution of the mixed layer in the Subantarctic Zone south of Australia. J. Geophys. Res. 106, 31463–31487.

Rintoul, S.R., Donguy, J.-R., Roemmich, D.H., 1997. Seasonal evolution of upper ocean thermal structure between Tasmania and Antarctica. Deep-Sea Res., Part I 44, 1185–1202.

Rintoul, S.R., Hughes, C., Olbers, D., 2002a. The Antarctic Circumpolar System. In: Siedler, G., Church, J., Gould, J. (Eds.), Ocean Circulation and Climate. Academic Press (in press).

Rintoul, S.R., Sokolov, S., Church, J.A., 2002b. A six year record of austral summer baroclinic transport variability of the Antarctic Circumpolar Current at 140E, derived from XBT and altimeter measurements. J. Geophys. Res. (in press).

Rosenberg, M., Eriksen, R., Rintoul, S., 1995a. Aurora Australis marine science cruise AU9309/AU9391: oceanographic field measurements and analysis. Res. Rep., vol. 2. Antarct. Coop. Res. Cent., Hobart, Tasmania, Australia, 103 pp.

Rosenberg, M., Eriksen, R., Bell, S., Bindoff, N., Rintoul, S., 1995b. Aurora Australis marine science cruise AU9407: oceanographic field measurements and analysis. Res. Rep., vol. 6. Antarct. Coop. Res. Cent., Hobart, Tasmania, Australia, 97 pp.

Rosenberg, M., Eriksen, R., Bell, S., Rintoul, S., 1996. Aurora Australis marine science cruise AU9404: oceanographic field measurements and analysis. Res. Rep., vol. 8. Antarct. Coop. Res. Cent, Hobart, Tasmania Australia, 53 pp.

Rosenberg, M., Bray, S., Bindoff, N., Rintoul, S., Johnson, N., Bell, S., Towler, P., 1997. Aurora Australis marine science cruise AU9501, AU9604, and AU9601: Oceanographic field measurements and analysis, inter-cruise comparisons and data quality notes. Res. Rep., vol. 12. Antarct. Coop. Res. Cent., Hobart, Tasmania, Australia, 150 pp.

Sievers, H.A., Nowlin Jr., W.D., 1984. The stratification and water masses at Drake Passage. J. Geophys. Res. 89, 10489–10514.

Sokolov, S., Rintoul, S.R., 2001. The subsurface structure of Southern Ocean surface temperature anomalies. J. Geophys. Res. (submitted for publication).

Sparrow, M.D., Heywood, K.J., Brown, J., Stevens, D.P., 1996. Current structure of the south Indian ocean. J. Geophys. Res. 101, 6377–6392.

Trull, T.W., Rintoul, S.R., Hadfield, M., Abraham, E.R., 2001. Circulation and seasonal evolution of polar waters south of Australia: implications for iron fertilization of the Southern Ocean. Deep-Sea Res., Part II 48 (11–12), 2439–2466.

Whitworth, T., 1980. Zonation and geostrophic flow of the Antarctic Circumpolar Current at Drake Passage. Deep-Sea Res., Part A 27, 497–507.